Christie, D.M., Pedersen, R.B., Miller, D.J., et al., 2001
Proceedings of the Ocean Drilling Program, Initial Reports Volume 187

1. Leg 187 Summary[1]

Shipboard Scientific Party[2]

ABSTRACT

Leg 187 undertook to trace the boundary between Indian and Pacific, ocean-scale mantle provinces across 10- to 30-Ma seafloor of the Southeast Indian Ocean between Australia and Antarctica. The boundary is sharply defined on young seafloor within the Australian Antarctic Discordance (AAD), where it is migrating to the west at ~40 mm/yr.

The leg was built around a responsive drilling strategy in which real-time shipboard geochemical analyses from one site were used to guide the selection of subsequent sites from a slate of preapproved targets. This strategy proved highly effective, allowing us to maximize our time on site and to focus on sites that could potentially yield the best definition of the boundary configuration. Using Ba and Zr contents of basalt glasses referenced to our database of younger (0–7 Ma) lavas from the AAD and Zone A (east of the AAD), we were able to assign each of the 23 holes drilled at 13 sites to an Indian, Pacific, or Transitional-Pacific upper mantle type. At three sites we encountered lavas from two of these three mantle types, indicating mixed or transitional mantle sources.

From these shipboard identifications of mantle domain, three fundamental observations can be made:

1. No Indian-type mantle occurs east of the regional residual depth anomaly.
2. Pacific- and especially Transitional-Pacific–type mantle occurs throughout the depth anomaly in the study area.
3. Between ~28 and 14 Ma, Indian and Pacific mantle types alternated in western Zone A on a time scale of a few million years.

These observations lead to the following tentative conclusions which require careful testing as isotopic data become available. A discrete man-

[1]Examples of how to reference the whole or part of this volume.
[2]Shipboard Scientific Party addresses.

Ms 187IR-101

tle boundary comparable to the present-day boundary in the AAD cannot be mapped through the entire 14- to 28-Ma time interval encompassed by Leg 187 sites, although comparable boundaries have existed for relatively short, discrete time intervals. We conclude that, in the long term, the eastern limit of the Indian mantle province corresponds closely to the eastern edge of the residual depth anomaly. Its locus must lie close to the –500-m residual depth contour that tracks south to connect with the known location of the Indian/Pacific boundary on younger seafloor of the AAD. West of this boundary, sporadic occurrences of Transitional-Pacific–type and even Pacific-type mantle are interspersed with the predominant Indian-type mantle. The western limit of Pacific or Transitional-Pacific mantle is not closely defined by our data, but it is most likely associated with the western boundary of the depth anomaly. The alternation of Indian-type sites with Pacific- and Transitional-Pacific–type sites in western Zone A on time scales of a few million years can be interpreted in terms of discrete incursions, either of Indian mantle beneath Zone A or, perhaps more likely, of Pacific mantle into the dominantly Indian region of the depth anomaly.

Samples from Leg 187 will undergo extensive elemental and isotopic analysis to refine the definition of the isotopic boundary and to improve our understanding of the nature and origin of the AAD, the mantle boundary, and the distinctive Indian Ocean mantle province. In addition, a battery of samples collected as quickly as possible under conditions that were as sterile as possible were placed in a variety of media in order to characterize the microbial population of the deep seafloor. Complementary electron microscope studies will seek to characterize fossil and living microbes involved with biodegradation of basaltic glass and their habitats.

INTRODUCTION

Background

Indian and Pacific Mantle Isotopic Provinces

Lavas erupted at Indian Ocean spreading centers are isotopically distinct from those of the Pacific Ocean, reflecting a fundamental difference in the composition of the underlying upper mantle. Along the Southeast Indian Ridge (SEIR), the Indian Ocean and Pacific Ocean mantle isotopic provinces are separated by a uniquely sharp boundary (Klein et al., 1988). This boundary has been located to within 25 km along the spreading axis of the SEIR within the Australian Antarctic Discordance (AAD) (Pyle et al., 1992; Christie et al., 1998). Subsequent off-axis dredge sampling has shown that Pacific mantle has migrated rapidly westward during at least the last 4 m.y. The principal objective of Leg 187 was to delineate this boundary farther off axis, allowing us to infer its history over the last 30 m.y.

Australian Antarctic Discordance

The AAD (Fig. F1) is a unique region, encompassing one of the deepest (4–5 km) regions of the global mid-oceanic spreading system. Its anomalous depth reflects the presence of unusually cold underlying mantle and, consequently, of thin crust (Marks et al., 1990; Forsyth et al., 1987; Sempéré et al., 1991; West et al., 1994). Despite a uniform, in-

F1. Southeast Indian Ocean regional map with Leg 187 operational area and possible isotopic boundary configurations, p. 19.

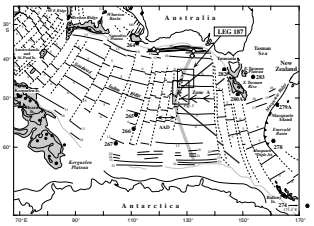

termediate spreading rate, the SEIR undergoes an abrupt morphologic change across the eastern boundary of the AAD (Palmer et al., 1993). The region east of the AAD, known as Zone A, is characterized by an axial ridge with relatively smooth off-axis topography (characteristics usually associated with fast-spreading centers), whereas the AAD, also known as Zone B, is characterized by deep axial valleys with rough off-axis topography (characteristics usually associated with slow-spreading centers). Other anomalous characteristics of the AAD include a pattern of relatively short axial segments separated by long transforms with alternating offset directions, unusually thin oceanic crust, chaotic seafloor terrain dominated by listric extensional faulting rather than magmatism, high upper mantle seismic wave velocities, and an intermittent asymmetric spreading history (Weissel and Hayes, 1971, 1974; Forsyth et al., 1987; Marks et al., 1990; Sempéré et al., 1991; Palmer et al., 1993; West et al., 1994; West, 1997; Christie et al., 1998). The morphological and geophysical contrasts across the eastern boundary of the AAD are paralleled by distinct contrasts in the nature and variability of basaltic lava compositions (Pyle, 1994), reflecting fundamental differences in magma supply because of strong contrasts in the thermal regime of the spreading center.

Mantle Flow and the Isotopic Boundary

The AAD appears to be the locus of converging asthenospheric mantle flows. This is suggested by multiple episodes of ridge propagation from both east and west toward the AAD (Vogt et al., 1984; Cochran et al., 1997; Sempéré et al., 1997; Sylvander, 1998; West et al., 1999) and by recent numerical model studies suggesting that significant convergent subaxial mantle flow is an inevitable consequence of gradients in axial depth and upper mantle temperature around the AAD (West and Christie, 1997; West et al., 1999).

Within Segment B5, the easternmost AAD segment, a distinct discontinuity in the Sr, Nd, and Pb isotopic signatures of axial lavas marks the boundary between Indian Ocean and Pacific Ocean mantle provinces (Klein et al., 1988; Pyle et al., 1990, 1992). The boundary is remarkably sharp, although lavas with transitional characteristics occur within 50–100 km of the boundary (Fig. **F2**). Along the axis of the SEIR, the boundary is located within 20–30 km of the ~126°E transform, the western boundary of Segment B5. The boundary has migrated westward across Segment B5 during the last 3–4 m.y. (Pyle et al., 1990, 1992; Christie et al., 1998).

Although the recent history of this uniquely sharp boundary between ocean basin–scale upper mantle isotopic domains has been reasonably well defined by mapping and conventional dredge sampling, its long-term relationship to the remarkable geophysical, morphological, and petrological features of the AAD had not been determined prior to Leg 187. The AAD is a long-lived major tectonic feature (Veevers, 1982). Its defining characteristic is its unusually deep bathymetry, which stretches across the ocean floor from the Australian to the Antarctic continental margins. The trend of this depth anomaly forms a shallow, west-pointing V-shape, cutting across the major fracture zones that currently define the eastern AAD segments (Figs. **F1, F3**). This V-shape implies that the depth anomaly has migrated westward at a long-term rate of ~15 mm/yr (Marks et al., 1991), which is much slower than either the recent migration rate of the isotopic boundary or the majority of the known propagating rifts along the SEIR (i.e., 25–30 mm/yr).

F2. Along-axis profiles of isotopic ratios and bathymetry from the AAD, p. 20.

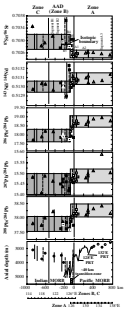

F3. Possible isotopic boundary configurations, p. 21.

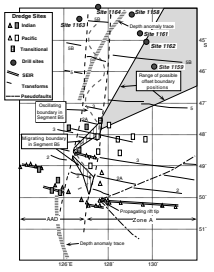

Further, the relatively rapid northward absolute motion of the SEIR requires that the mantle "source" of the depth anomaly be linear and oriented approximately north-south. Recently, Gurnis et al. (1998) have suggested that the source of this cold linear anomaly lies in a band of subducted material that accumulated at the 660-km mantle discontinuity beneath a long-lived western Pacific subduction zone before ~100 Ma.

History of the Isotopic Boundary

Prior to Leg 187, the locus and history of the isotopic boundary before ~4 Ma were almost completely unknown. Possible long-term relationships between the isotopic boundary and the morphologically defined AAD could be divided into two distinct classes (schematically illustrated in Fig. F3). Either the recent (0–4 Ma) isotopic boundary migration simply reflects a localized (~100 km) perturbation of a geochemical feature that has been associated with the eastern boundary of the AAD since the basin opened, or the migration is a long-lived phenomenon that only recently brought Pacific mantle beneath the AAD. In the first case, the boundary could be related either to the depth anomaly or to the eastern bounding transform but not, in the long term, to both. The second possibility, that the isotopic boundary only recently arrived beneath the AAD, was first proposed by Pyle et al. (1992), building on a suggestion by Alvarez (1982, 1990), that Pacific mantle began migrating westward when the South Tasman Rise first separated from Antarctica at 40–50 Ma. Limited geochemical support for this hypothesis came from the Indian and transitional isotopic signatures of altered ~38- and ~45-Ma basalts dredged to the north and east of the AAD by Lanyon et al. (1995) and from 60- to 69-Ma Deep Sea Drilling Project (DSDP) basalts that were drilled close to Tasmania (Pyle et al., 1995). Unfortunately, neither sample set is unequivocal. The dredged samples are from sites within the residual depth anomaly and therefore support two of the three possible configurations. The DSDP samples lie far to the east of the depth anomaly but very close to the continental margin. Their apparent Indian affinity is suspect because of the possibility that their mantle source has been contaminated by nearby subcontinental lithosphere. Finally, the oldest (~7 Ma) off-axis dredge sample from Zone A is of Pacific type (Christie et al., 1998), constraining possible loci of the Indian/Pacific boundary to intersect the eastern AAD transform north of approximately 47°45′S.

Objectives

Locating the Isotopic Boundary

The principal objective of Leg 187 was to locate the Indian/Pacific mantle boundary through its expression in the geochemistry of mid-ocean-ridge basalt (MORB) lavas from 8- to 28-Ma seafloor to the north of the AAD. The clearest definition of this boundary can be seen in the Pb isotopic ratios, but it is clear in Sr and apparent in Nd isotopic ratios as well (Fig. F2). Although there are also clear overall differences in the major and trace element compositions between the lava populations of the two provinces, there are few elements that can reliably determine the mantle source affinity of individual lavas. Two elemental plots that can assign >90% of our current collection of young lavas are Zr/Ba vs. Ba and Na_2O/TiO_2 vs. MgO (see "Mantle Domain Recognition," p. 13,

in "Geochemistry"). These elements were measured by inductively coupled plasma–atomic emission spectroscopy (ICP-AES) aboard the *JOIDES Resolution* throughout the leg. The Ba and Zr systematics appear to enable us to discriminate between basalts of Pacific affinity and their Indian and transitional counterparts, but Na_2O/TiO_2 proved to be less useful for this purpose because the boundary between Indian and Pacific types appears to be at lower Na_2O/TiO_2 values for the Leg 187 samples (see "Geochemistry" and "Summary" in the site chapters).

Beyond the Isotopic Boundary

In addition to its interest as a mantle dynamics phenomenon, an improved understanding of the Indian/Pacific mantle boundary is important for a broader general understanding of the oceanic mantle. In investigating the nature and origins of the AAD, the isotopic boundary and the mantle provinces that it separates, we are also investigating the importance of variations in geochemistry, isotopic composition, temperature, and other physical characteristics of the oceanic upper mantle in a setting where spreading rate is constant. Improved knowledge of the distribution of these chemical and physical characteristics in space and time will lead to a better understanding of the dynamics of the oceanic mantle and of its interaction with the magmatic processes of the mid-ocean-ridge system.

Subsurface Biosphere

Recent findings have extended the known biosphere to include microbial life in deep subsurface volcanic regions of the ocean floor, and much attention has been focused on the nature of microbes that live on, and contribute to the alteration of, basaltic glass in oceanic lavas (Thorseth et al., 1995; Furnes et al., 1996; Fisk et al., 1998; Torsvik et al., 1998). The first evidence for this phenomenon was from textures in basaltic glass from Iceland (Thorseth et al., 1992). Similar textures were later found in basaltic glass from Ocean Drilling Program (ODP) Hole 896A at the Costa Rica Rift, and the microbial contribution to the alteration history was supported by the presence of DNA along the assumed biogenic alteration fronts (Thorseth et al., 1995; Furnes et al., 1996; Giovannoni et al., 1996). Microbes have recently been documented to inhabit internal fracture surfaces of basaltic glasses that were sampled specifically for microbiological studies during *MIR* submersible dives to the Knipovich Ridge (Thorseth et al., 1999). Dissolution textures directly beneath and manganese and iron precipitates adjacent to many individual microbes suggest that microbial activity plays an active role in the low-temperature alteration of ocean-floor basalts.

Rock and sediment samples collected during Leg 187 for microbial culturing, DNA analysis, and electron microscopic study range in age from 14 to 28 Ma, providing an opportunity to study temporal changes in microbial alteration.

Drilling Strategy

In order to fulfill the primary objective of the leg (the location and characterization of the Indian/Pacific mantle isotopic boundary), our drilling strategy was focused on maximizing the number of sites rather than recovery or penetration at any one site. Although our goal for each site was ~50 m penetration into basaltic basement, this was

achieved only at five sites. At most sites, drilling conditions were poor as we penetrated broken pillow flows, talus, or other rubble, and many holes were abandoned when they became unstable.

Much of the region is devoid of measurable sediment cover. Most sites were located on localized sediment pockets detected by single-channel seismic (SCS) imaging during the *R/V Melville* site survey cruises Boomerang 5 and Sojourner 5. Three additional sites were surveyed during the transit from Site 1158 to 1159, and two of these were subsequently drilled as Sites 1161 and 1162. Based on the seismic records, all sites were ranked on a scale of 1 to 3, depending on the clarity with which they were imaged and the width and depth of sediment cover. At highly ranked sites, sediment thickness predictions from site survey data proved to be reasonably accurate, so, whenever possible, we chose higher ranked sites. At Site 1152, only a few meters of soft sediment were encountered, and spud-in conditions were little better than those for bare rock. Two other low-ranked sites, AAD-2b and -3a (Sites 1159 and 1163), proved to have more than adequate sediment cover and were drilled successfully.

As the *JOIDES Resolution* approached each site, we ran a short survey using the 3.5-kHz precision depth recorder and, in all but a few cases, the SCS system to confirm the location and suitability of the proposed site. Whenever possible, these surveys were run obliquely to the original north-south survey lines, but in some cases weather conditions dictated that we run close to the original course. For several smaller sites we chose to run north-south lines to minimize out-of-plane reflections from the dominantly east-west trending topography.

Because sediments across the region were expected to be reworked and possibly winnowed and because basement penetration at as many sites as possible was the primary objective of this leg, we chose in most cases to wash through the sediment section. Wash cores containing significant sediment intervals were recovered at 10 sites. Site locations and data are summarized in Table T1.

T1. Coring summary, Leg 187, p. 47.

During Leg 187 we used a responsive drilling strategy. At key points during the leg, subsequent sites were chosen from among the 19 preapproved sites according to the results of onboard geochemical analysis of the recovered basalts. Details of the analytical program and its use to distinguish Indian from Pacific mantle signatures can be found in "Geochemistry," p. 11, and in the individual site summaries.

IGNEOUS PETROLOGY

Introduction

During Leg 187 we drilled 617 m of volcanic basement, recovering 137 m of core. By far the dominant lithology recovered was pillow basalt, either as pillow flows or as basaltic rubble. Also common were basaltic breccias cemented by various types of sedimentary infill, including carbonates, clays, and lithic debris. Massive basalts were interlayered with pillow flows at Site 1160. Hole 1162A is anomalous, as greenschist facies metadiabase, metagabbro and cataclasite were recovered as clasts in a dolomite-cemented lithic breccia, suggesting that deeper crustal levels have been exposed nearby. All other holes sampled only the uppermost volcanic carapace. Virtually all the recovered basalts have been pervasively altered, with Fe oxyhydroxide and clay as the typical alteration products. At all but two sites, we washed through

100–200 m of sediment, recovering at most a few meters in wash barrels. Both clay- and carbonate-rich sediments were encountered. Lithified sediments are present just above the volcanic basement in some holes, with highly varying amounts recovered. The rock types recovered during Leg 187 are summarized in Table T2, and brief descriptions of the typical lithologies are given below.

T2. Igneous petrology summary, p. 48.

Pillow Basalt and Basaltic Rubble

Pillow basalts were sampled in all cores both as intact pillow lava and as rubble. Pillow fragments are recognized in the core by their curved chilled margins, radial fracture patterns, and V-shaped piece outlines (Fig. F4). Chilled margins are common in most cores; more than 170 glassy margins were sampled by the science party for postcruise studies. Typically, chilled margins are composed of an outer, 1- to 10-mm glassy rind that grades through a discrete spherulitic zone into a coalesced spherulitic zone. Such zones are commonly easily visible in hand specimen as the mesostasis has been turned light brown by alteration, highlighting the spherulitic texture. Many of the glassy rinds have attached veneers or crosscutting veins of interpillow sediment that is carbonate rich in some cases and clay rich in others.

F4. Pillow fragment with chilled margin and fracture-controlled morphology, p. 22.

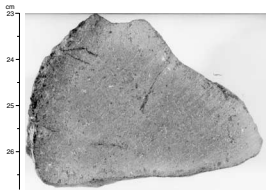

Basaltic rubble was recovered from 10 of 23 holes. The rubble is distinguished by multiple weathered surfaces that were not cut by the drill. Commonly, rubble fragments can be recognized as pillow basalt based on the criteria outlined above. In many holes rubble was encountered just below the contact between sediment and basalt, providing very poor drilling conditions and requiring that the initial hole be abandoned in 9 out of 13 sites. In those instances a second hole was started within 200 m; in all but one case (Site 1158), this second hole allowed us to satisfactorily complete our drilling objectives. In a few holes, rubble was encountered at a deeper level, below intact lava flows, demonstrating that at least some of the rubble deposits formed within the active volcanic zone.

Massive Basalt

Massive basalts, with recovered (i.e., minimum) thicknesses of as much as 1.5 m were recovered only from Hole 1160B. These can be distinguished by long (up to 50–60 cm), continuous core pieces with uniform texture (Fig. F5). In Hole 1160B each of the three massive basalts is overlain by a pillow flow of similar lithology. In one massive flow, olivine phenocrysts increase in abundance toward the base, suggesting that there has been some crystal settling. No chilled margins were recovered from the massive units. Site 1160 is the easternmost of the Leg 187 sites. It is located at the northern foot of a 1500-m-high seamount in the middle of Zone A. The abundance of massive flows at this site may reflect the generally robust magmatism of Zone A of the SEIR, or it may reflect increased magmatism related to the seamount itself.

F5. Fresh massive basalt core, p. 23.

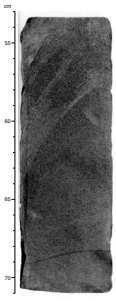

Interpillow Sediments and Basaltic Breccias

Basalts are intimately associated with sediments at 8 of the 13 sites. Sediment is present as interpillow fill, as fracture fill, and as both small clasts and matrix material in breccias of various types. Interpillow and fracture fills are common in Holes 1155B and 1163A, where micritic limestone is attached to (and infills fractures in) the glassy margins (Fig.

F6). Fracture infills extend deep into individual pieces, and they are typically made up of micritic sediment containing sand-sized or smaller glass/palagonite and basalt fragments. Subsequent diagenetic and wall-rock reactions, probably related to fluid flow through the fractures, have transformed the simple fracture fill to a composite, partly sedimentary, partly chemically precipitated vein fill.

The breccias can be subdivided into (1) volcanic breccias, formed during or soon after eruption, and (2) breccias that formed after extensive basalt alteration. The best examples of volcanic breccia are found in Holes 1159A, 1163A, and 1164B. Hyaloclastite breccia, consisting of angular to subrounded glass/palagonite in a clay matrix, was recovered from Hole 1159A, and hyaloclastite breccia with calcarenite to calcareous clay matrix is present in Hole 1163A. Rounded glass fragments included in the carbonate matrix suggest that some of the lava flows sampled in Hole 1159A erupted onto (or into) unconsolidated sediment. Volcanic breccia dominated by aphyric basalt and glass/palagonite clasts was sampled in Hole 1164B. This breccia differs from all other Leg 187 breccias in having only insignificant amounts of nonlithic sedimentary matrix.

Posteruptive, carbonate-cemented breccias are prominent in seven holes (Holes 1155B, 1156A, 1157A, 1161A, 1161B, 1162A, and 1162B). The multistage, posteruptive evolution of these breccias is evident in the common truncation by fracturing of alteration halos around the original clast margins and in the common occurrence of composite sediment-basalt clasts. Breccias of this type range from matrix supported (Fig. F7) to clast supported, with clast sizes varying from several tens of centimeters to a few millimeters. The carbonate-cemented basalt breccia from Hole 1156A had a particularly complex evolution: much of the clast material has a multistage alteration and fracturing history, and there are two generations of matrix carbonate (Fig. F8) followed by late-stage carbonate veining. The formation of this breccia must have involved deposition and redeposition of talus in a tectonically active setting, accompanied and followed by sediment deposition, lithification, and, ultimately, carbonate veining.

Dolomite-cemented basalt breccias were recovered from Holes 1162A and 1162B. In Hole 1162A, a polymict clast assemblage composed of greenschist facies metagabbro, metadiabase, basalt, and cataclasites is cemented by crystalline dolomite with a subsidiary fine lithic component that imparts variable bright red and green colors to the matrix. All the clasts in Hole 1162B are very highly altered basalts that have been transformed almost entirely to clay under low-temperature conditions.

Petrography of Basalts

Leg 187 basalts range from aphyric (Fig. F9) to moderately phyric (Fig. F10), with small vesicles, up to 1–2 mm in size, in a small proportion of the rocks. Plagioclase and olivine are the typical phenocryst phases, with plagioclase being most abundant. No systematic spatial or temporal variations in the abundances of phenocryst phases were observed. Cr spinel is present in accessory amounts as small, euhedral inclusions in plagioclase and olivine phenocrysts or as discrete subhedral crystals as large as 0.5 mm. Clinopyroxene phenocrysts and microphenocrysts are present only in Holes 1152B and 1164A. These holes are located in Segments B4 and B5 near the western margin of the depth anomaly. At the spreading axis, these zones are characterized by relatively unevolved lavas with a high degree of compositional variability

F6. Micritic limestone infilling a fracture and interpillow space, p. 24.

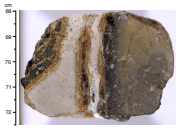

F7. Poorly sorted basaltic breccia, p. 25.

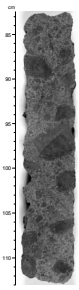

F8. Basalt and palagonitized glass clasts in calcareous sediment matrix, p. 26.

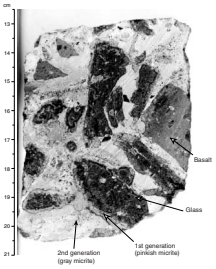

F9. Microcrystalline aphyric basalt, p. 27.

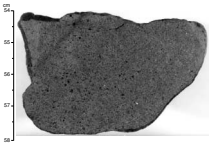

F10. Moderately plagioclase-olivine phyric pillow basalt, p. 28.

for a given MgO content. These characteristics suggest an array of primary magma compositions, with minimal mixing and differentiation at crustal levels. The presence of clinopyroxene phenocrysts at these sites, in lavas of relatively high MgO content, may reflect high-pressure fractionation within these more magma-starved segments.

As many as 30% of the phenocrysts are glomerocrysts. These range from centimeter-sized loose clusters of prismatic plagioclase and equant olivine (Fig. F11) to tightly intergrown aggregates. Corroded xenocrysts and xenocrystic aggregates are present in several samples from different cores; disequilibrium textures, including discontinuous zoning and sieve-textures (Fig. F12), are common in the larger plagioclase phenocrysts (Fig. F13).

Groundmass textures in the pillow basalts are typically microcrystalline, ranging from intersertal to sheaf quench crystal morphologies. Groundmass is usually dominated by acicular to skeletal plagioclase, with equant, often skeletal, olivine forming in subordinate amounts. Clinopyroxene occurs predominantly as plumose quench growths (Fig. F14) or as bundles of bladed crystals, but larger, anhedral to euhedral, granular to prismatic, crystals occur adjacent to and within miarolitic cavities in several holes. The massive flows in Hole 1160B show intergranular to subophitic groundmass textures (Fig. F15).

ALTERATION

All basalts recovered during Leg 187 have been subjected to low-temperature alteration. Macroscopically, alteration is manifested most commonly as alteration halos (1) around the margins of pieces and (2) following veins and open fractures. There is a broad range of alteration intensity within and between sites, from completely fresh, to incipient iron staining, to pervasive discoloration. Alteration phases replacing phenocrysts and groundmass include abundant Fe oxyhydroxides and clay minerals, with common cryptocrystalline silica and Mn oxide encrustations. Less commonly, carbonate has replaced groundmass and precipitated along veins. At one site, greenschist facies assemblages were recovered.

Low-Temperature Alteration

Phenocrysts and Groundmass

Distinctive concentric low-temperature alteration halos commonly follow the shapes of the outer surfaces of individual basalt pieces. On cut surfaces, these halos mimic the extent of red-brown alteration on exterior facets of pieces that show no evidence of drilling abrasion, suggesting that many of the pieces recovered were basaltic rubble accumulated in the sedimented valleys that we, of necessity, selected as drilling targets. However, at several sites, we recovered drill-cut, contiguous pieces showing the normal progression from palagonitized glassy margins, through altered zones of discrete and/or coalesced spherulites, to holocrystalline basalt (Figs. F16, F17), indicating that intact pillows were sampled.

Alteration halos on core pieces usually have sharp, smooth contacts with the less altered piece interiors (Fig. F18), although some are gradational and/or irregular. At most sites, several zones can be distinguished in these alteration rinds, progressing from more intensely altered rims

F11. Plagioclase + olivine glomerocryst, p. 29.

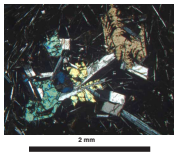

F12. Sieve-textured plagioclase, p. 30.

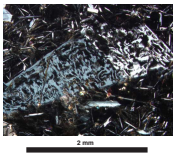

F13. Euhedral plagioclase phenocrysts in basalt, p. 31.

F14. Clinopyroxene plumose quench texture, p. 32.

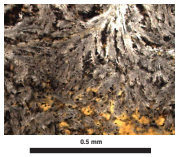

F15. Subophitic texture, p. 33.

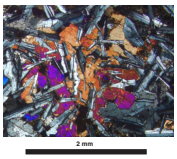

F16. Fractures lined with cryptocrystalline silica within chilled pillow margin, p. 34.

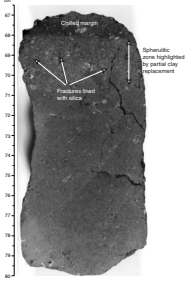

where Fe oxyhydroxides and clay pervasively replace groundmass and phenocrysts alike, to less intensely altered areas where only groundmass phases are altered.

In at least some pieces from every site, low-temperature alteration is pervasive. This alteration is developed as brown-red discoloration of the entire piece, apparent on drill-cut exteriors of pieces as well as on the cut faces of cores. In these pieces the groundmass and most phenocrysts are altered to Fe oxyhydroxide and clay, although fresh kernels are common. In both alteration halos and pervasively altered pieces, olivine phenocrysts are much more intensely altered than plagioclase. Fe oxyhydroxide and clays commonly only highlight cleavage planes, fractures, and crystal margins in plagioclase.

The most widespread evidence of low-temperature alteration seen in thin section is partial to complete replacement of quench textured phases and mesostasis by Fe oxyhydroxide and clay (Fig. F19). Crystalline groundmass phases are variably altered through replacement of olivine, clinopyroxene, and mesostasis to smectite and Fe oxyhydroxide, visible as a pervasive or patchy discoloration and cloudy appearance. Groundmass plagioclase is usually fresh or incipiently altered.

Olivine phenocrysts are commonly completely altered, or nearly so, to clay, Fe oxyhydroxide, and magnetite. In some sections, olivine pseudomorphs show euhedral grain shapes, but only the cores of grains are preserved. In others, olivine alteration is restricted to fractures. The main alteration product of plagioclase is Fe oxyhydroxide, mostly along cleavage planes and fractures. Plagioclase is rarely completely replaced; in nearly every thin section there is more fresh than altered plagioclase.

Overall alteration characteristics vary from site to site. Basalts from Sites 1152, 1153, and 1154 are only slightly altered, expressed as minor replacement of groundmass and phenocrysts by secondary phases. This is interesting in that these are the oldest sites we drilled (~26 to 28 Ma). Alteration at Sites 1161 and 1162, associated with a westward propagating rift, are dominated by carbonate- and/or silica-cemented breccias, and both show moderate to high degrees of alteration. Angular basalt clasts in the breccias are commonly pervasively altered, and at least some of the alteration occurred prior to brecciation, as evidenced by truncated alteration halos. Hole 1164B, which sampled only basaltic rubble, shows the most pervasive effects of alteration. More than 50% of clasts at this site are pervasively altered, deep brown in color, with only a few plagioclase microphenocrysts remaining unaltered. All other sites showed a range of slight to moderate alteration, less intense overall than Sites 1161, 1162, and 1164, although we recovered at least a few pieces of pervasively altered basalt at every site. The effects of alteration on bulk rock composition are discussed in "Introduction," p. 11, in "Geochemistry."

Glass

Palagonitized pillow rinds ranging in thickness from 0.5 to 10 mm were sampled at every site. Fresh, black, basaltic glass is common, surrounded by ubiquitous yellow to orange palagonite that is in places crosscut by a network of anastomosing silica (Fig. F20) and, more rarely, silica and calcite veins. Fresh glass and palagonite commonly occur in thin (0.5–2 mm), irregularly interlayered sheets, with palagonite being most abundant (>90%) in the outermost sections. In thin section, altered glass rims show weak parallel banding, except at the alteration front, along which dendritic features extending into fresh glass are be-

F17. Spherulitic pillow margin highlighted by Fe oxyhydroxide staining, p. 35.

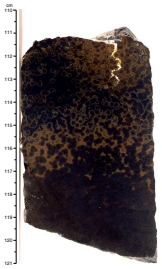

F18. Concentric alteration halos, p. 36.

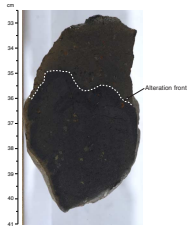

F19. Transition from smectite and Fe oxyhydroxide groundmass replacement to unaltered groundmass, p. 37.

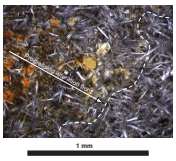

F20. Glassy pillow rind, p. 38.

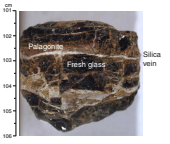

lieved to be related to microbial degradation (Thorseth et al., 1995) (Fig. F21).

Veins

Veins are present in all the cores. They include both compositionally homogeneous and composite veins, as well as rare crack-seal veins. Veins filled with combinations of silica, Fe oxyhydroxide, clay, and Mn oxide are present at every site, whereas calcite-bearing veins were only observed at Sites 1153, 1155, 1156, 1157, 1160, and 1163. The most common carbonate-bearing vein assemblage includes thin (<1 mm) linings of cryptocrystalline silica along vein selvages, spotted with sporadic submillimeter Mn oxide, accompanied by fillings of microcrystalline to cryptocrystalline calcite (Fig. F22). Additionally at these sites, composite veins commonly change from silica filled within the palagonitized glass and chilled margins to calcite filled toward the pillow interiors. Sites 1160 and 1162 are the only sites where chlorite is a common vein-filling phase. Dolomite veins are present only at Site 1162. Sediment-filled fractures are common in breccia clasts and pillow lavas that retain adhered interpillow sediment. At Site 1156, sediment-filled fractures and the breccia matrix contain two generations of calcite: (1) early, pink micritic calcite that is the dominant sedimentary component of the breccia matrix, and (2) late, sparry calcite precipitated along fractures and in void spaces.

Metamorphism

At Site 1162, a number of breccia clasts have higher temperature metamorphic mineral assemblages. Macroscopically, both aphyric and phyric basalts are greenish brown, strikingly different in color from any other rocks recovered during Leg 187. Olivine phenocrysts are completely replaced by Fe oxyhydroxide and a pale yellow combination of chlorite, talc, and clay. In clasts of lower metamorphic grade, groundmass olivine and clinopyroxene are extensively replaced by Fe oxyhydroxide and clay in most pieces, and several pieces have a chloritized groundmass. The presence of chlorite indicates that these rocks underwent metamorphism at 150°–250°C (Alt et al., 1996).

A few pieces of gabbro, diabase, or cataclasite at this site have developed greenschist facies mineral assemblages. Fibrous actinolite and chlorite have replaced clinopyroxene, and olivine is totally replaced by concentric layers of talc, chlorite, and magnetite. Plagioclase is partially replaced by clay and chlorite and is recrystallized to albite along grain margins. Thin veins (<1 mm) are filled with chlorite and clay. The occurrence of actinolite, talc, chlorite, and albite in upper crustal basalts is consistent with lower greenschist facies metamorphism (Alt et al., 1996).

GEOCHEMISTRY

Introduction

The rapid-turnaround shipboard analytical capability provided by the new ICP-AES instrument was fundamental to the success of Leg 187. At several points throughout the leg, data from one site were used in deciding which of two or even three alternate plans would be fol-

F21. Intersection of calcite veins with palagonite, p. 39.

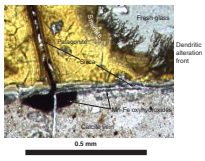

F22. Calcite veins, p. 40.

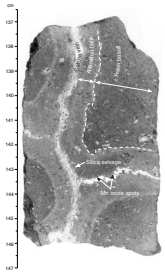

lowed for the succeeding few sites. This reactive strategy enabled us to rapidly determine that the isotopic boundary is closely related to the eastern side of the regional depth anomaly. We were then able to focus with confidence on sites in the vicinity of the depth anomaly, to the exclusion of sites in eastern Zone A.

The Indian/Pacific mantle boundary was originally identified within the AAD on the basis of isotopic ratios in seafloor lavas, and these ratios, particularly $^{206}Pb/^{204}Pb$, continue to be the only definitive discriminants between Pacific and Indian mantle provinces (Fig. **F23**). In planning for Leg 187, we worked exhaustively with our data from zero-age and young (<7 Ma) dredge samples throughout the AAD and Zone A to identify a reliable discriminant that could be analyzed on board the *JOIDES Resolution*. A single element, barium, appeared to be both reliable as a discriminant and relatively easy to determine with the necessary accuracy. For ease of use, we settled upon a single diagram, Zr/Ba vs. Ba, as providing a clear, visual discrimination between Indian- and Pacific-type lavas from our 0- to 7-Ma data set. A second element ratio, Na/Ti (expressed as Na_2O/TiO_2 throughout this report), also appeared to have potential as a discriminant, although both elements are susceptible to fractionation by a variety of magmatic processes. As it turned out, the 0- to 7-Ma dividing line on this diagram does not apply to most Leg 187 sites, so we relied almost exclusively on Ba-Zr systematics in our decision-making process. We recognize, however, that the Ba-Zr systematics may be an imperfect discriminant and that some sites could have been misidentified as Indian or Pacific type. In addition, some Leg 187 samples occupy a field (referred to as Transitional Pacific) not represented among our 0- to 7-Ma samples (see "Mantle Domain Recognition," below). Therefore shipboard determinations of mantle domain will remain tentative until isotope data become available.

The glasses from Leg 187 sites are all relatively primitive with MgO ranging from 9.4 to 7.2 wt%. With few exceptions, whole-rock samples have significantly lower MgO contents than the associated glasses. At the most extreme, whole-rock MgO values are lower by 3–4 wt%, but in most cases they are lower by only 0.5–1.0 wt%. These variations in MgO are seldom accompanied by coherent variations in other elements; therefore, they cannot be attributed to crystallization or other magmatic processes. A particularly clear example of this phenomenon is provided by Hole 1160B, which recovered seven lithologic units, three of which are massive flows interspersed with pillow flows. Each massive flow is overlain by a pillow flow of the same lithology. Whole-rock samples from all three massive flows and glasses from two of the overlying pillow flows are essentially identical in composition with ~8.9–9.1 wt% MgO (Fig. **F24**). Whole rocks from the pillow flows, however, have lower MgO contents, differing from the glasses by as much as 3–4 wt%. Most other elements in the pillow whole-rock samples are similar in abundance to the glass and massive flow samples. We conclude from these observations that MgO is selectively removed from pillow interiors as a result of the pervasive low-temperature alteration that has affected all our sites.

Element concentrations and variations other than Ba, Zr, Ti, Na, and MgO have received only cursory examination and discussion at most sites. However, significant differences are apparent in parental magma composition between Leg 187 lavas and present-day lavas from the same segment. For Segments B4 and B5, these variations are likely related to the westward migration of the depth anomaly relative to the

F23. Variations in $^{206}Pb/^{204}Pb$ along the SEIR in the AAD and of Zr/Ba vs. $^{206}Pb/^{204}Pb$, p. 41.

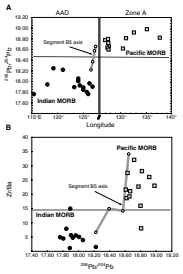

F24. Distribution of MgO values in Hole 1160B, p. 42.

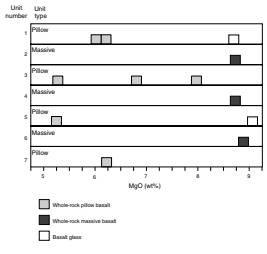

segment boundaries. In Zone A, temporal variability appears to have been modulated by repeated rift propagation.

Mantle Domain Recognition

Barium and Zirconium

Throughout Leg 187, we used ICP-AES Ba and Zr data to determine mantle domain based on the 0- to 7-Ma data fields in the Zr/Ba vs. Ba diagram. Because of the potential for alteration of Ba content by seawater alteration, we used only hand-picked basalt glasses in making this determination. Figure F25 shows all available glass data from the AAD region. There is a clear division between glasses from the Indian mantle domain and those from the Pacific domain. A tie line connecting all the glasses from the transitional domain beneath the Segment B5 axis cuts across both fields (e.g., Segment B5 axis; Fig. F25). The only 0- to 7-Ma lavas that do not fall within the clearly defined Indian and Pacific fields are a small group of primitive lavas from propagating rift tips in Zone A.

Leg 187 glass data are plotted in relation to the 0- to 7-Ma Ba-Zr fields and the Segment B5 tie line in Figure F26A. Although many of the Leg 187 data plot within or very close to the 0- to 7-Ma fields and can readily be assigned to one of these fields, there is an important group of data that cannot. These data plot in the area below the Pacific field (i.e., toward lower Zr/Ba values and slightly higher Ba content than the majority of Pacific-type lavas). We refer to these lavas as Transitional-Pacific type because they appear to represent an extension of the Pacific field toward the compositions of the Zone A propagating rift tip lavas (Fig. F26A). This extension may reflect a temporal shift in any of several source parameters, including source composition and overall extent of melting or a shift in the mixing proportions of one or more mantle end-member components. It could also reflect addition of Ba to the samples from seawater, either directly by low-temperature alteration or indirectly by assimilation of altered crust into the magma. In terms of the Zr/Ba vs. Ba diagram, basaltic liquids plotting in the Transitional-Pacific field could also have been derived by crystal fractionation from Indian-type parents. We would expect this to produce trends that cut across the observed data array at a high angle. The data do not, however, support a fractionation origin for the Transitional-Pacific glasses, as there is no apparent progression to decreasing MgO across the Indian field or into the Transitional-Pacific field. Finally, lavas from the Transitional-Pacific field are distinct from transitional lavas along the Segment B5 tie line and are therefore unlikely to reflect mixing between Indian and Pacific domains as is presently defined by Segment B5 axial lavas.

Sodium and Titanium

For the 0- to 7-Ma glasses, a plot of Na_2O/TiO_2 values vs. MgO content effectively discriminates Indian-domain glasses from those of the Pacific domain, again with the Segment B5 tie line spanning the divide between domains (Fig. F25B). Unfortunately, this diagram does not apply in a straightforward way to the Leg 187 glasses. In Figure F26B, Leg 187 glass data are plotted on this diagram and coded as Indian, Pacific, or Transitional Pacific according to their position on the Zr/Ba vs. Ba diagram (Fig. F26A). According to this division, no Leg 187 Indian-type

F25. Variations in Zr/Ba vs. Ba content of basaltic glass and variations in Na_2O/TiO_2 values vs. MgO content of 0- to 7-Ma basaltic glass, p. 43.

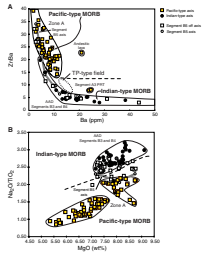

F26. Leg 187 shipboard glass analyses in relation to the 0- to 7-Ma data fields, p. 44.

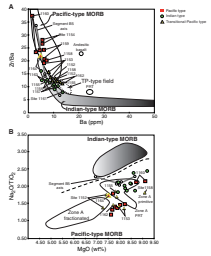

lava plots in the 0- to 7-Ma "Indian" field, and lavas of all three types are intermixed in the "Pacific" field.

Although it is offset to lower Na_2O/TiO_2 than the 0- to 7-Ma field, Leg 187 Indian lavas do define a discrete field, although this field also encompasses several Transitional-Pacific and Pacific lavas. The three Pacific lavas are, however, all from Site 1160; these also have the three lowest Ba contents of the Leg 187 Pacific lavas. In Figure F26A, they plot to the left of the Segment B5 tie line. The only other sample with comparable low Ba content is the borderline Pacific sample from Site 1164 that is plotted as a red triangle in the figure.

This offset of the Pacific/Indian field boundary appears to reflect the generally low Na_2O contents of Leg 187 glasses relative to those of the AAD. Whether this apparently fundamental shift in primary magma chemistry reflects a temporal change in mantle temperature and/or extent of melting, a change in source composition or some other source parameter cannot be evaluated without further data.

Distribution of Mantle Domains

Most of the Leg 187 sites are distributed along three north-south transects, one each in Segments B4 and B5 and one in western Zone A (Figs. F27, F28). There are two additional sites in eastern Zone A.

Segments B4 and B5

Indian-type mantle was present beneath all three Segment B5 sites and one Segment B4 site (1163) at their time of eruption. At two sites, basalts derived from two distinct mantle types were erupted in close proximity. Glasses from Hole 1155A are of Transitional-Pacific type, whereas those from Hole 1155B, 200 m away, are of Indian type. Glasses from Holes 1164A and 1164B are of Pacific and Indian types, respectively, although the Pacific-type glass plots very close to the boundary between the two fields. (This glass is represented by a red triangle in Fig. F26A.) Only Transitional-Pacific–type glass was recovered at Site 1152.

Zone A West

Six sites form a transect between crustal ages 28 and 14 Ma in western Zone A (Figs. F27, F28). Along this transect, Indian-type mantle was present at ~23 and 19 Ma, but in three out of four cases the transition between Indian and Pacific type is constrained to have taken place within no more than 2–3 m.y. The fourth transition, north of Site 1157, is not constrained as there is no site in this area.

Zone A East

Sites 1154 and 1160 in eastern Zone A are distinctly of Pacific type (Figs. F27, F28).

Summary

Taking the shipboard identifications of mantle domain at face value, three fundamental observations can be made:

F27. Site locations in relation to seafloor isochrons, p. 45.

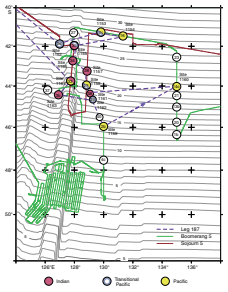

F28. Site locations in relation to the residual depth anomaly and SeaBeam bathymetry, p. 46.

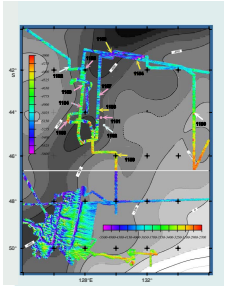

1. No Indian-type mantle occurs east of the –500-m contour on the regional depth anomaly. At ~6 Ma, this contour is very close to the rough/smooth terrain boundary that marks the isotopic boundary in Segment B5 (Fig. F28).
2. Pacific- and especially Transitional-Pacific–type mantle occurs sporadically throughout the region of the depth anomaly, at least in the older part of the study area.
3. Between ~25 and 14 Ma, Indian- and Pacific-type mantle alternated in western Zone A on a time scale of a few million years, comparable in time scale to the recent migration of Pacific-type mantle across Segment B5.

From these observations we draw the following tentative conclusions, which will require careful testing as the isotopic data become available.

A discrete mantle boundary comparable to the present-day boundary in the AAD cannot be mapped through the entire 14- to 28-Ma time interval encompassed by Leg 187, although comparable boundaries may have existed for relatively short time intervals. For the longer term, it appears likely that the eastern limit of the Indian-mantle province corresponds closely to the eastern edge of the depth anomaly. The locus of this boundary is unconstrained, but it must lie close to the –500-m residual depth contour. West of this boundary and perhaps coinciding with the deepest region of the depth anomaly (–500 m), Indian mantle predominates, but occurrences of Transitional-Pacific– and even Pacific-type mantle are not uncommon. The western limit of Pacific- or Transitional-Pacific–type mantle is not well defined by our data, but it cannot be farther east than the –400-m residual depth contour on the west side of the depth anomaly.

The alternation of Indian-type sites with Pacific- and Transitional-Pacific–type sites along the western Zone A transect from 14 to 25 Ma suggests a rapid alternation of discrete mantle types on time scales of a few million years, comparable in time scale to the recent (0–4 Ma) migration in the AAD. These occurrences can be interpreted as discrete incursions, possibly of Indian mantle beneath Zone A, but more likely of Pacific-type mantle into the dominantly Indian region of the depth anomaly. If either interpretation is correct, then a discrete Indian/Pacific boundary likely existed for much of that time.

Transitional-Pacific–type mantle is not represented in our 0- to 7-Ma data set, and we have interpreted it as an extension of the Pacific-mantle field rather than a transition between the Pacific- and Indian-type domains as defined by present-day SEIR MORB glass. This type may manifest a mantle component that cannot be seen in the well-mixed, high-flux magma systems of Zone A. In the region of the depth anomaly, magma flux is greatly reduced and small magma batches with a variety of individual source signatures may be erupted with little modification.

CONCLUSION

By any measure, Leg 187 was highly successful. We recovered samples from 23 holes at 13 sites with an average water depth of almost 5 km. In the process, a record 140 km of drill string was passed through the drill floor. In part, this success relates to the unusually mild weather that we encountered. In larger part, it relates to the extraordinary dedication of the *JOIDES Resolution* and ODP crews. Our reactive drilling

strategy worked well. After limited teething troubles with sample preparation and running of the new ICP-AES instrument, we were able to obtain the geochemical data that we needed within 12 hr of "core on deck" for critical samples.

Our principal objective was to determine the configuration of the Indian/Pacific mantle isotopic boundary beneath 10- to 30-Ma seafloor north of the AAD. Using the shipboard Ba and Zr data, we believe that we have outlined the boundary with some precision. Confirmation of our interpretations (and the fulfillment of our objective) will require onshore isotopic analyses. The discrete isotopic boundary that has migrated across Segment B5 of the AAD over the last 3 to 4 m.y. is probably not a permanent feature, but we have tentatively identified two similar migration events in western Zone A at about 19 and 22 Ma. Over the long term, the Indian/Pacific boundary is probably represented by a transitional region that coincides with the regional depth anomaly. This region appears to be dominated by Indian-type mantle with discrete occurrences of Transitional-Pacific– and even, rarely, Pacific-type mantle. In western Zone A, along the eastern boundary of the depth anomaly, Pacific- and Indian-type mantle domains appear to alternate on a time and spatial scale that is comparable to the present-day migration in Segment B5. This alternation may represent short-lived incursions of Indian mantle beneath Zone A, but incursions of Pacific mantle into the depth anomaly are more likely by analogy with present-day evidence for mantle migration and because Pacific mantle is associated with robust magmatism.

Samples from Leg 187 will undergo extensive geochemical and isotopic analysis onshore. Initially, these studies will serve to confirm the mantle provenance of the lavas that we sampled and refine our understanding of the location and nature of the mantle isotopic boundary. Further study will allow us to better understand changes (1) in mantle composition, temperature, and dynamics; (2) in melting conditions; and (3) in magma evolution. Comparative studies with other regions worldwide will enable us to improve our understanding of the nature of both mantle domains and of the origin and evolution of the depth anomaly and the AAD.

Although results will not be available for some time, the microbiology objectives of the leg have been well served. Between two and six samples were taken at each site. The samples include a range of lithologies, including pillow rims, pillow interiors, massive flows, and various breccias. The samples also vary in the extent and type of alteration. Samples will be cultured in a variety of media, at low and high pressures. Electron microscope studies will attempt to characterize living and fossil microbes and their habitats.

REFERENCES

Alt, J.C., Laverne, C., Vanko, D.A., Tartarotti, P., Teagle, D.A.H., Bach, W., Zuleger, E., Erzinger, J., Honnorez, J., Pezard, P.A., Becker, K., Salisbury, M.H., and Wilkens, R.H., 1996. Hydrothermal alteration of a section of upper oceanic crust in the eastern equatorial Pacific: a synthesis of results from Site 504 (DSDP Legs 69, 70, and 83, and ODP Legs 111, 137, 140, and 148.) *In* Alt, J.C., Kinoshita, H., Stokking, L.B., and Michael, P.J. (Eds.), *Proc. ODP, Sci. Results,* 148: College Station, TX (Ocean Drilling Program), 417–434.

Alvarez, W., 1982. Geological evidence for the geographical pattern of mantle return flow and the driving mechanism of plate tectonics. *J. Geophys. Res.,* 87:6697–6710.

——— , 1990. Geologic evidence for the plate driving mechanism: the continental undertow hypothesis and the Australian-Antarctic Discordance. *Tectonics,* 9:1213–1220.

Cande, S.C., LaBrecque, J.L., Larson, R.L., Pitmann, W.C., III, Golovchenko, X., and Haxby, W.F., 1989. Magnetic lineations of the world's ocean basins. *AAPG Map Ser.,* 131 (scale 1:27,400,000).

Christie, D.M., West, B.P., Pyle, D.G., and Hanan, B., 1998. Chaotic topography, mantle flow and mantle migration in the Australian-Antarctic Discordance. *Nature,* 394:637–644.

Cochran, J.R., Sempéré, J.-C., Christie, D.M., Eberle, M., Feli, L., Goff, J., Kimura, H., Ma, Y., Shah, A., Small, C., Sylvander, B., West, B., and Zhang, W., 1997. The Southeast Indian Ridge between 88°E and 118°E: gravity anomalies and crustal accretion at intermediate spreading rates. *J. Geophys. Res.,* 102:15463–15487.

Fisk, M.R., Giovannoni, S.J., and Thorseth, I.H., 1998. Alteration of oceanic volcanic glass: textural evidence of microbial activity. *Science,* 281:978–980.

Forsyth, D.W., Ehrenbard, R.L., and Chapin, S., 1987. Anomalous upper mantle beneath the Australian-Antarctic Discordance. *Earth Planet. Sci. Lett.,* 84:471–478.

Furnes, H., Thorseth, I.H., Tumyr, O., Torsvik, T., and Fisk, M.R., 1996. Microbial activity in the alteration of glass from pillow lavas from Hole 896A. *In* Alt, J.C., Kinoshita, H., Stokking, L.B., and Michael, P.J. (Eds.), *Proc. ODP, Sci. Results,* 148: College Station, TX (Ocean Drilling Program), 191–206.

Giovannoni, S.J., Fisk, M.R., Mullins, T.D., and Furnes, H., 1996. Genetic evidence for endolithic microbial life colonizing basaltic glass/seawater interfaces. *In* Alt, J.C., Kinoshita, H., Stokking, L.B., and Michael, P.J. (Eds.), *Proc. ODP, Sci. Results,* 148: College Station, TX (Ocean Drilling Program), 207–214.

Gurnis, M., Muller, R.D., and Moresi, L., 1998. Cretaceous vertical motion of Australia and the Australian-Antarctic Discordance. *Science,* 279:1499–1504.

Klein, E.M., Langmuir, C.H., Zindler, A., Staudigel, H., and Hamelin, B., 1988. Isotope evidence of a mantle convection boundary at the Australian-Antarctic Discordance. *Nature,* 333:623–629.

Lanyon, R., Crawford, A.J., and Eggins, S., 1995. Westward migration of Pacific Ocean upper mantle into the Southern Ocean region between Australia and Antarctica. *Geology,* 23:511–514.

Marks, K.M., Sandwell, D.T., Vogt, P.R., and Hall, S.A., 1991. Mantle downwelling beneath the Australian-Antarctic Discordance Zone: evidence from geoid height versus topography. *Earth Planet. Sci. Lett.,* 103:325–338.

Marks, K.M., Vogt, P.R., and Hall, S.A., 1990. Residual depth anomalies and the origin of the Australian-Antarctic Discordance Zone. *J. Geophys. Res.,* 95:17325–17337.

Palmer, J., Sempéré, J.-C., Christie, D.M., and Phipps-Morgan, J., 1993. Morphology and tectonic of the Australian-Antarctic Discordance between 123°E and 128°E. *Mar. Geophys. Res.,* 15:121–151.

Pyle, D.G., 1994. Geochemistry of mid-ocean-ridge basalt within and surrounding the Australian Antarctic Discordance. [Ph.D. dissert.]. Oregon State Univ., Corvallis.

Pyle, D.G., Christie, D.M., and Mahoney, J.J., 1990. Upper mantle flow in the Australian-Antarctic Discordance. *Eos,* 71:1388. (Abstract)

————, 1992. Resolving an isotopic boundary within the Australian-Antarctic Discordance. *Earth Planet. Sci. Lett.,* 112:161–178.

Pyle, D.G., Christie, D.M., Mahoney, J.J., and Duncan, R.A., 1995. Geochemistry and geochronology of ancient southeast Indian and southwest Pacific seafloor. *J. Geophys. Res.,* 100:22261–22282.

Sempéré, J.-C., Palmer, J., Christie, D.M., Morgan, J.P., and Shor, A., 1991. Australian antarctic discordance. *Geology,* 19:429–432.

Sempéré, J.-C., Cochran, J.R., Christie, D.M., Eberle, M., Feli, L., Goff, J., Kimura, H., Ma, Y., Shah, A., Small, C., Sylvander, B., West, B., and Zhang, W., 1997. The Southeast Indian Ridge between 88° and 118°E: variations in crustal accretion at a constant spreading rate. *J. Geophys. Res.,* 102:15489–15505.

Sempéré, J.-C., Palmer, J., Phipps-Morgan, J., Christie, D.M., and Shor, A.N., 1991. The Australian-Antarctic Discordance. *Geology,* 19:429–432.

Sylvander, B.A., 1998. The Southeast Indian Ridge: water contents of MORB glasses and chemical effects of propagating rifts [M.S. thesis]. Oregon State Univ., Corvallis.

Thorseth, I.H., Furnes, H., and Heldal, M., 1992. The importance of microbiological activity in the alteration of natural basaltic glass. *Geochim. Cosmochim. Acta,* 56:845–850.

Thorseth, I.H., Pedersen, R.B., Daae, F.L., Torsvik, V., Torsvik, T., and Sundvor, E., 1999. Microbes associated with basaltic glass from the Mid-Atlantic Ridge. *Conf. Abstr., EUG 10,* Strasbourg, 4:254.

Thorseth, I.H., Torsvik, T., Furnes, H., and Muehlenbachs, K., 1995. Microbes play an important role in the alteration of oceanic crust. *Chem. Geol.,* 126:137–146.

Torsvik, T., Furnes, H., Muehlenbachs, K., Thorseth, I.H., and Tumyr, O., 1998. Evidence for microbial activity at the glass-alteration interface in oceanic basalts. *Earth Planet. Sci. Lett.,* 162:165–176.

Veevers, J.J., 1982. Australian-Antarctic depression from the mid-ocean ridge to adjacent continents. *Nature,* 295:315–317.

Vogt, P.R., Cherkis, N.K., and Morgan, G.A., 1984. Project Investigator-1: evolution of the Australian-Antarctic Discordance from a detailed aeromagnetic study. *In* Oliver, R.L., James, P.R., and Jago, J. (Eds.), *Antarctic Earth Science: Proc. 4th Inter. Symp. Antarctic Earth Sci.:* Canberra (Aust. Acad. Sci.), 608–613.

Weissel, J.K., and Hayes, D.E., 1971. Asymmetric seafloor spreading south of Australia. *Nature,* 231:518–522.

————, 1974. The Australian-Antarctic Discordance: new results and implications. *J. Geophys. Res.,* 79:2579–2587.

West, B.P., 1997. Mantle flow and crustal accretion in and near the Australian-Antarctic Discordance [Ph.D. thesis]. Univ. of Washington, Seattle.

West, B.P., and Christie, D.M., 1997. Diversion of along-axis asthenospheric flow beneath migrating ridge-transform-ridge intersections. *Trans. Am. Geophys. Union,* 78 (Suppl.):673.

West, B.P., Lin, J., and Christie, D.M., 1999. Forces driving ridge propagation. *J. Geophys. Res.,* 104:22845–22858.

West, B.P., Sempéré, J.-C., Pyle, D.G., Phipps-Morgan, J., and Christie, D.M., 1994. Evidence for variable upper mantle temperature and crustal thickness in and near the Australian-Antarctic Discordance. *Earth Planet. Sci. Lett.,* 128:135–153.

Figure F1. Regional map of the Southeast Indian Ocean (from Pyle et al., 1995) showing magnetic lineations (Cande et al., 1989), the Australian Antarctic Discordance (AAD), and Deep Sea Drilling Program (DSDP) sites (numbered solid circles) that sampled basement. Thin dark V east of the AAD = inferred trace of a hypothetical isotopic boundary migrating at ~40 mm/yr. Broader gray V = approximate trace of the regional depth anomaly. Bull's-eye symbols south of Australia = approximate positions of dredges by Lanyon et al. (1995). Darkly outlined box = area of operations for Leg 187; lighter outlined box = area of Figure F3, p. 21; small solid circles = DSDP and ODP site locations.

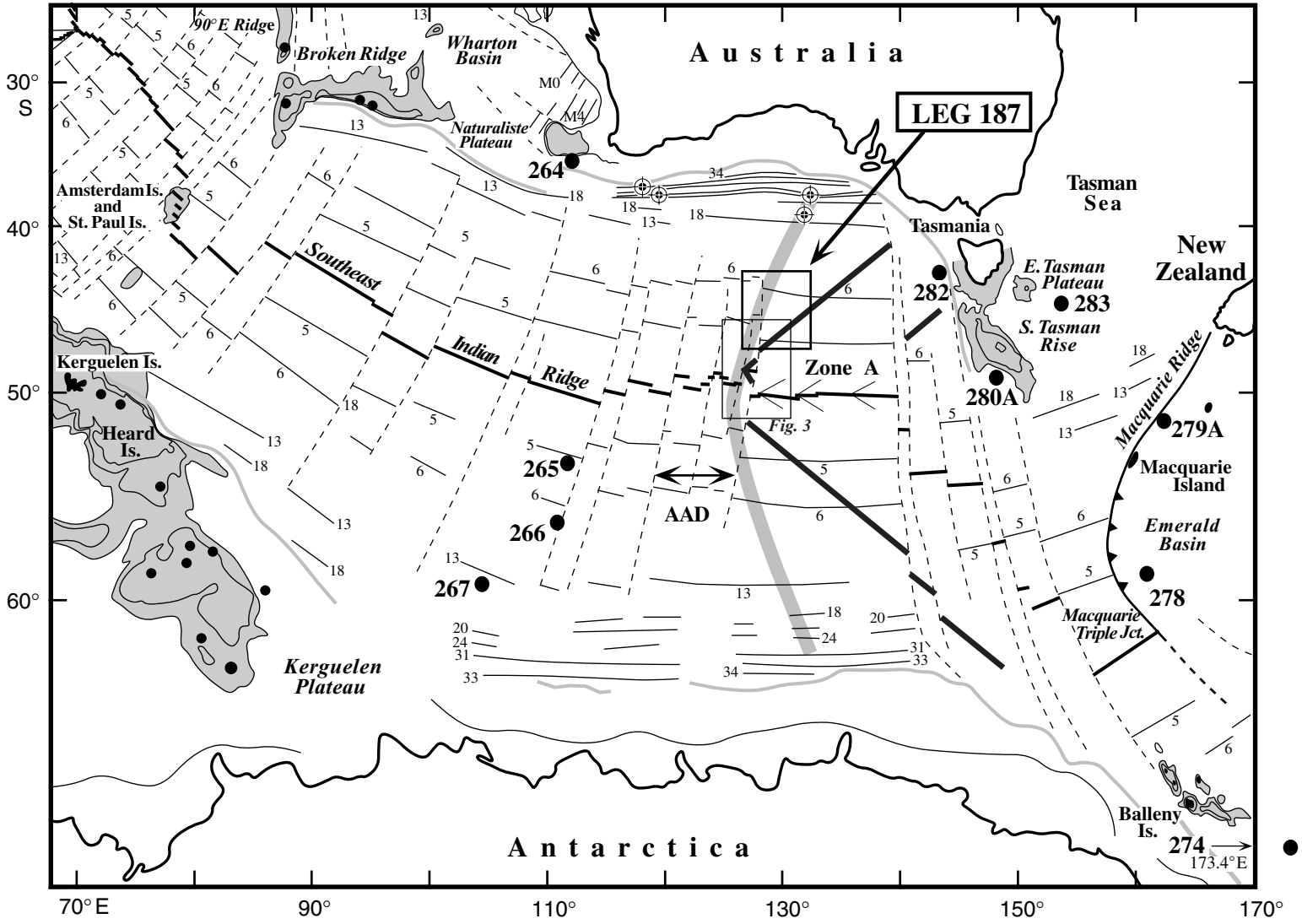

Figure F2. Along-axis profiles of isotopic ratios from the Southeast Indian Ridge between 114°E and 138°E. The horizontal scale is the distance from the eastern bounding (127°E) transform of the AAD. Open symbols and lightly shaded field = Pacific-type mid-ocean-ridge basalt (MORB); solid symbols and darker field = Indian-type MORB (from Pyle et al., 1992); triangles = data from Klein et al. (1988); squares = AAD data from Pyle et al. (1992). In the lowermost panel, solid circles = dredge depths; open circles = predicted axial depths from subsidence curves fit to flanks; and PRT = propagating rift tip.

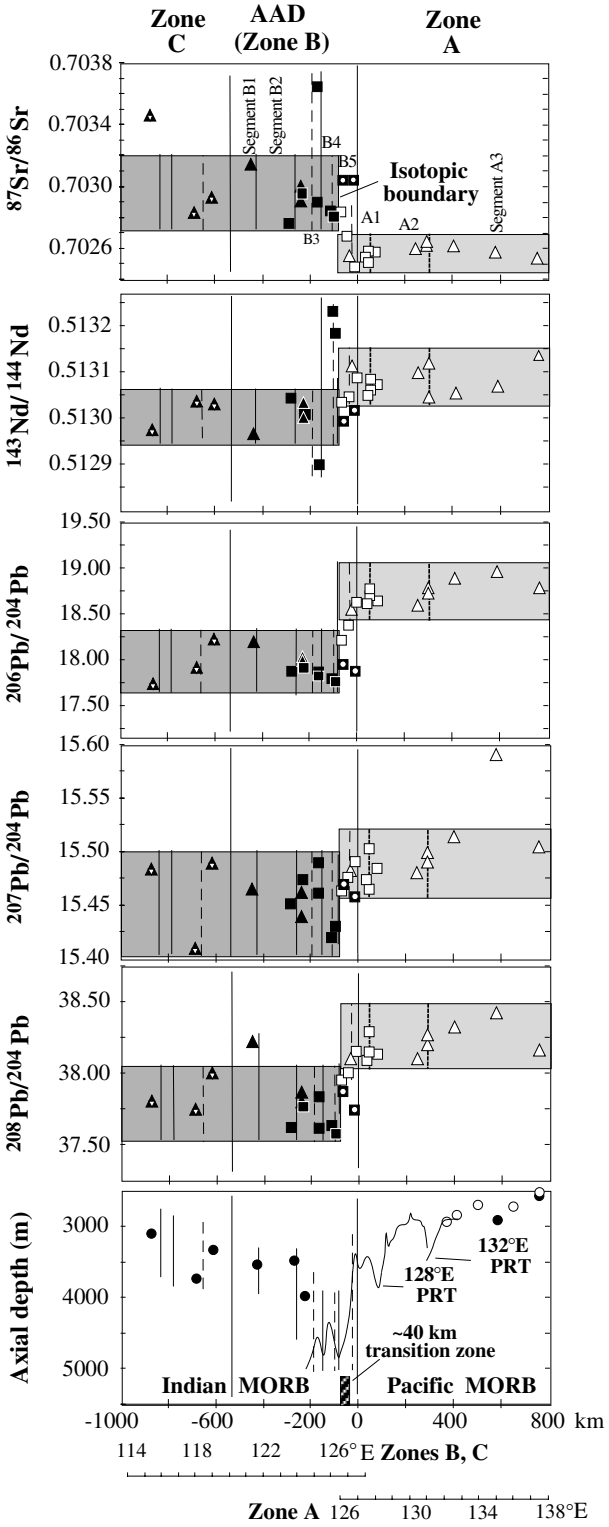

Figure F3. Isotopic boundary configurations allowed by pre-Leg 187 geochemical data from the dredge sites shown. Indian and Pacific populations are the same as those in Figure F2, p. 20. Migration across Segment B5 is confirmed, with the boundary constrained to the vertically ruled area labeled "Migrating boundary in Segment B5." East of the AAD, a hypothetical boundary produced by long-term westward migration is constrained to the medium-gray shaded region (upper right). Alternate boundary configurations are associated with the curving trace of the depth anomaly or oscillation between the easternmost AAD transforms. Dark gray solid circles = the more southerly Leg 187 sites. The remaining sites lie to the north and east of this map. Magnetic anomalies are numbered 2–5B. SEIR = Southeast Indian Ridge.

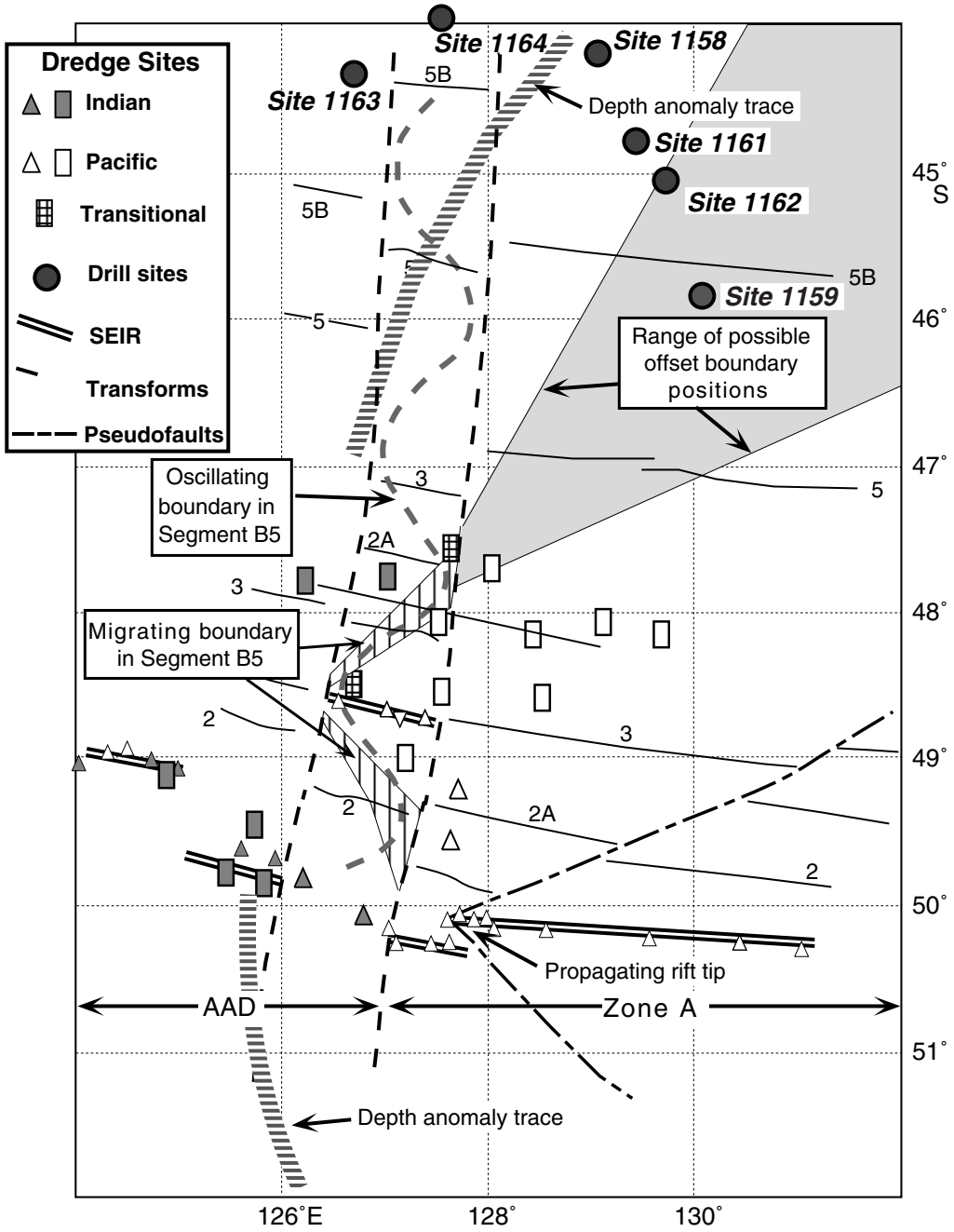

Figure F4. Photograph of interval 187-1164B-8R-1, 23–27 cm, showing a pillow fragment with its chilled margin along the left side and distinctive V-shaped, fracture-controlled morphology defined by the upper and lower (in the figure) surfaces.

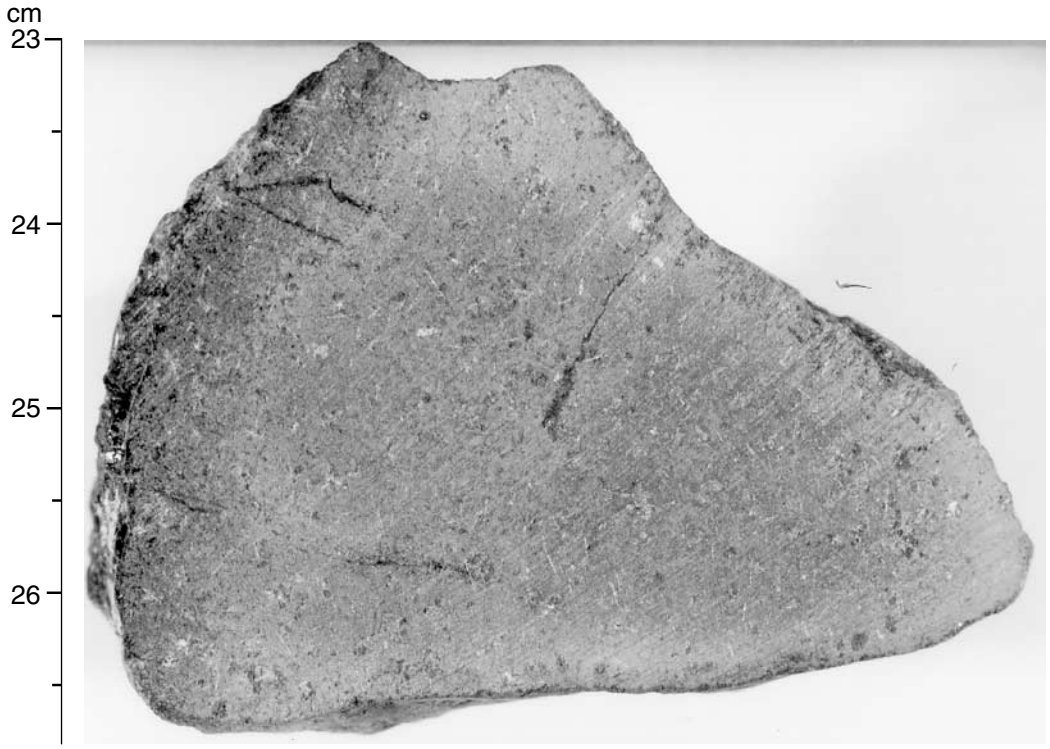

Figure F5. Photograph of interval 187-1160B-4R-2, 54–70 cm, showing a continuous core of fresh massive basalt.

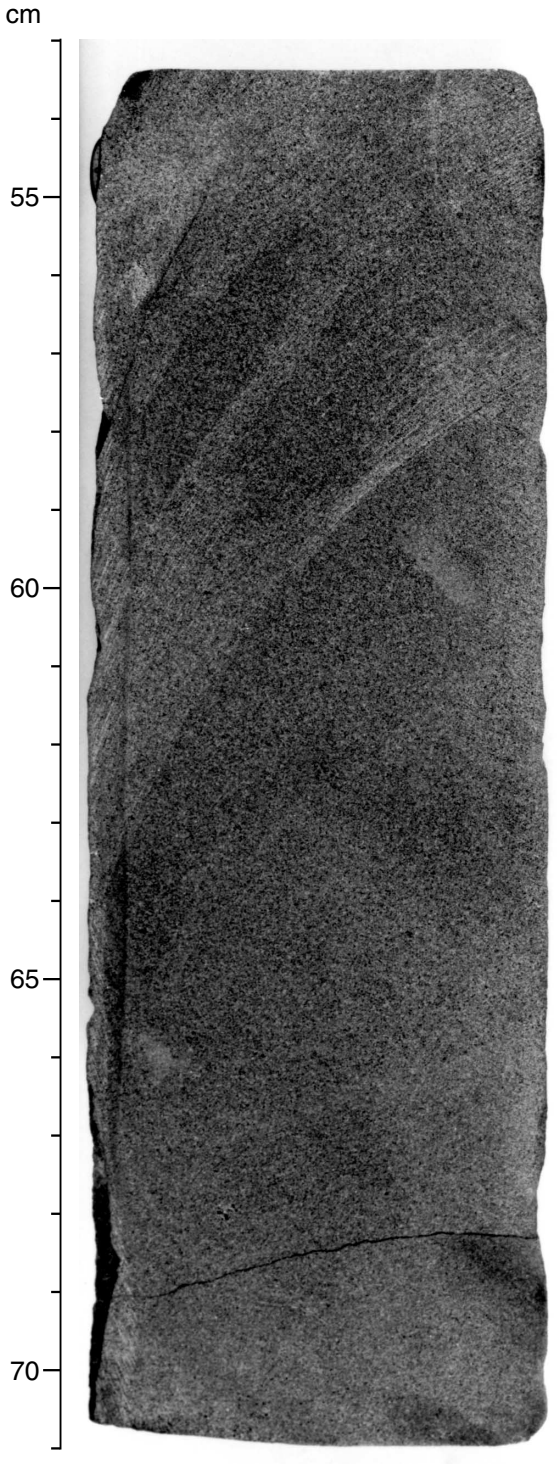

Figure F6. Photograph of interval 187-1155B-8R-3, 68–72 cm, showing micritic limestone infilling a fracture and interpillow space.

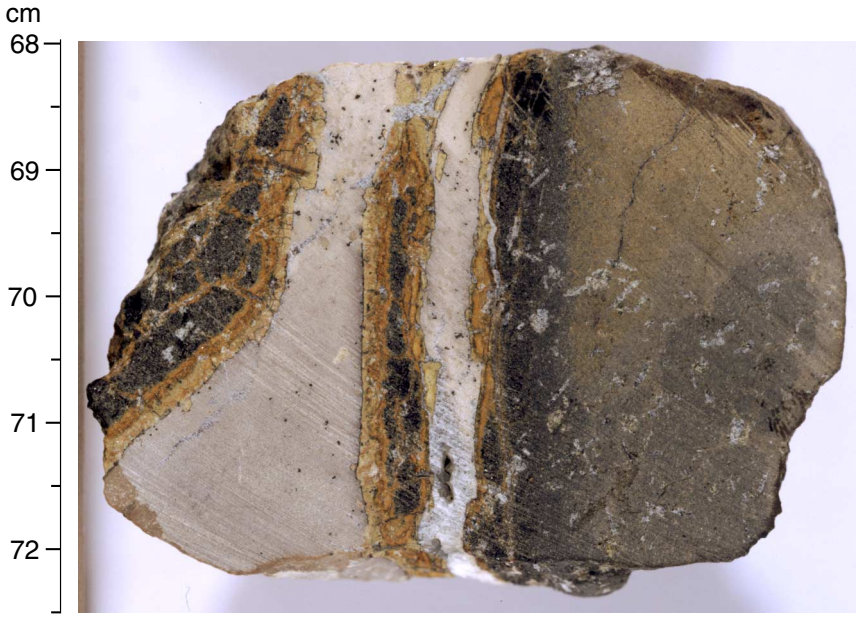

Figure F7. Photograph of interval 187-1161A-5R-1, 83–113 cm, showing poorly sorted basaltic breccia. Only basalt clasts are clearly visible.

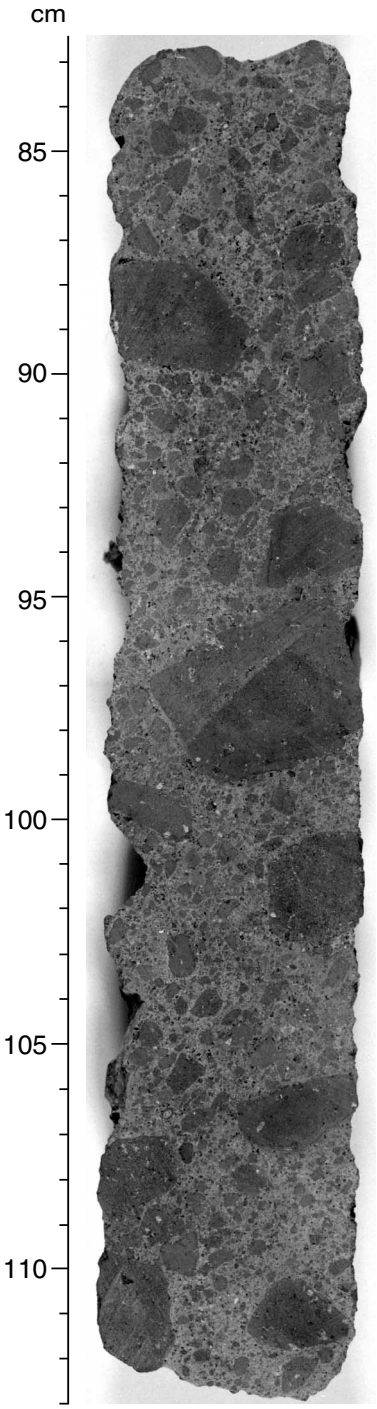

Figure F8. Photograph of interval 187-1156A-2R-2 (Piece 4, 14–20 cm), showing clasts of basalt and variably palagonitized glass in a two-stage calcareous sediment matrix.

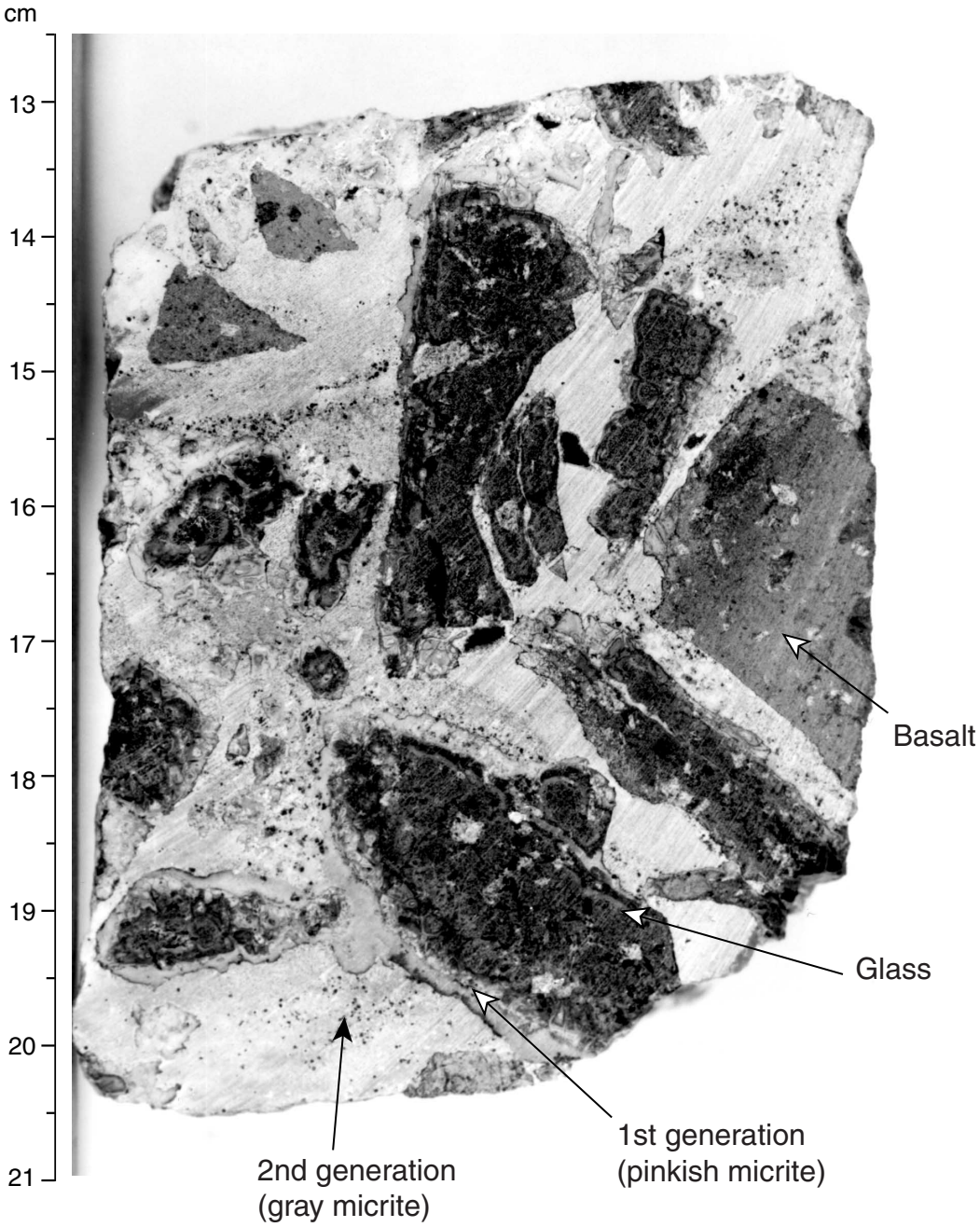

Figure F9. Photograph of interval 187-1161B-3R-1, 54–59 cm, showing microcrystalline aphyric basalt typical of Hole 1161B.

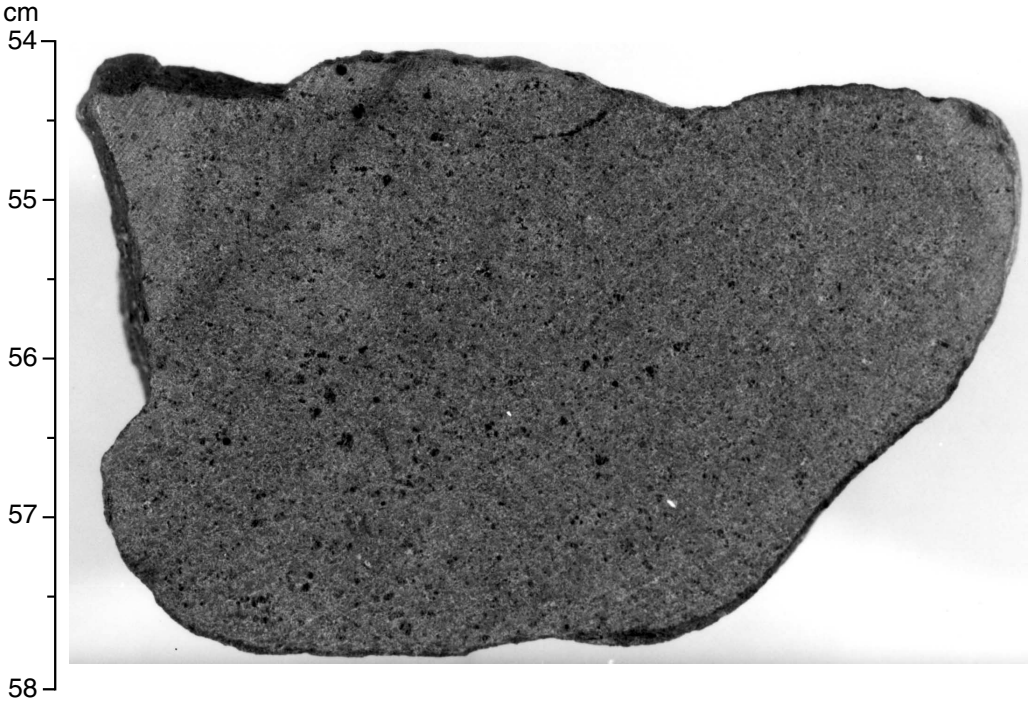

Figure F10. Photograph of interval 187-1154A-3R-1, 120–130 cm, showing light gray, moderately plagioclase-olivine phyric pillow basalt, typical of that recovered throughout Hole 1154A. Black irregular patches were formed by the plucking of altered groundmass from the cut surface.

Figure F11. Photomicrograph, with crossed polars, of Sample 187-1157B-6R-1, 43–47 cm (see "Site 1157 Thin Sections," p. 29), showing a glomerocryst of intergrown prismatic plagioclase and skeletal olivine phenocrysts in a glassy groundmass.

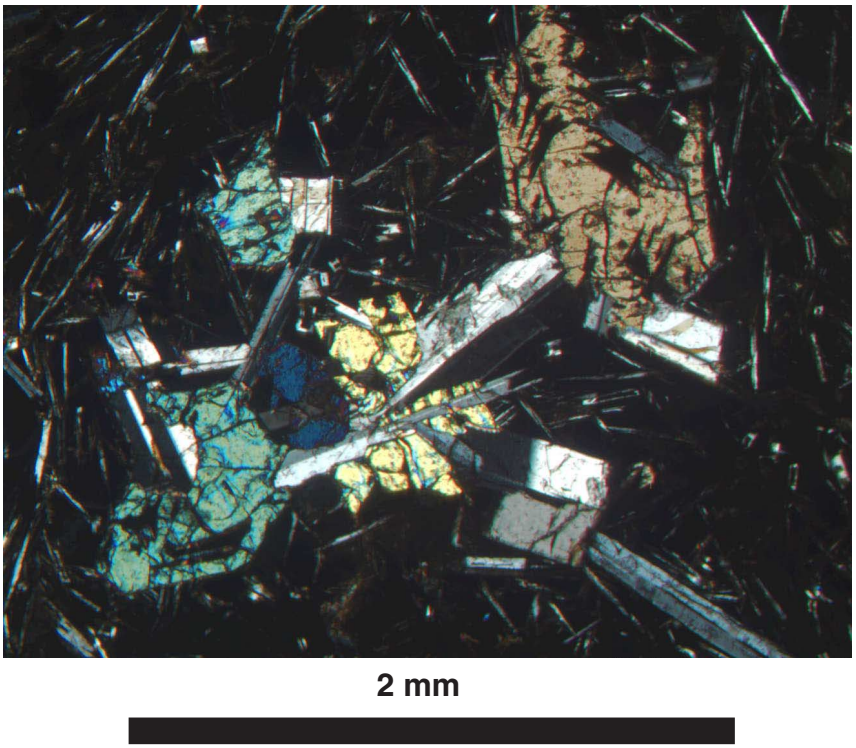

Figure F12. Photomicrograph, with crossed polars, of Sample 187-1164B-2R-1, 50–53 cm (see "Site 1164 Thin Sections," p. 22), showing sieve-textured plagioclase, indicative of partial resorption and disequilibrium with the host basalt.

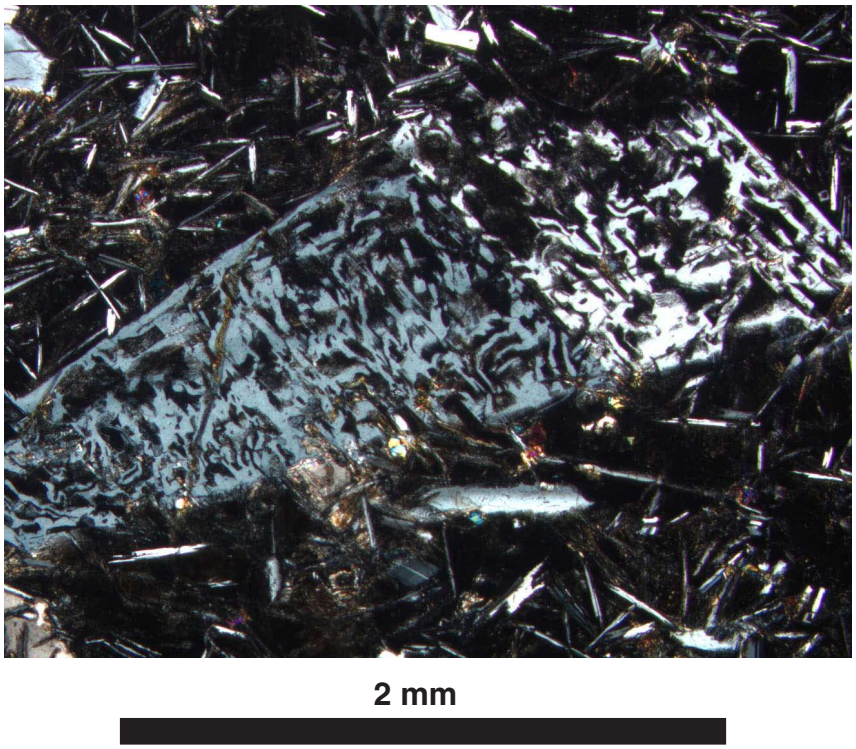

Figure F13. Photograph of interval 187-1152B-5R-1, 107–114 cm, showing large euhedral plagioclase phenocrysts in a sparsely plagioclase-olivine phyric basalt.

Figure F14. Photomicrograph, with crossed polars, of Sample 187-1152B-2R-1, 8–10 cm (see "Site 1152 Thin Sections," p. 10), showing clinopyroxene plumose quench texture. Note the replacement of groundmass mesostasis by smectite (lower right).

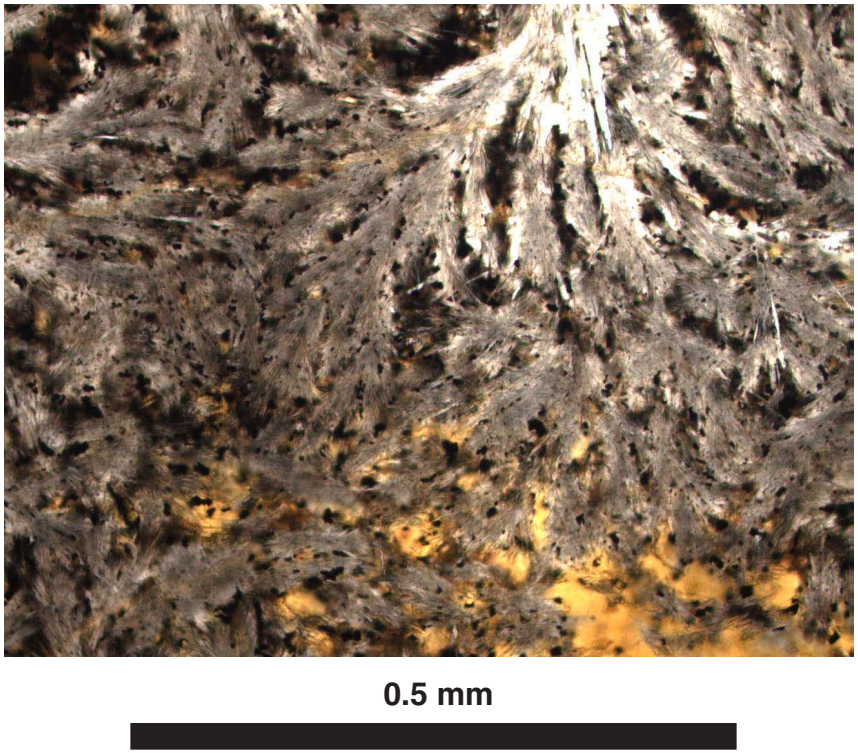

Figure F15. Photomicrograph, with crossed polars, of Sample 187-1158C-2R-1 (Piece 13, 75–78 cm) (see "Site 1158 Thin Sections," p. 16), displaying subophitic texture.

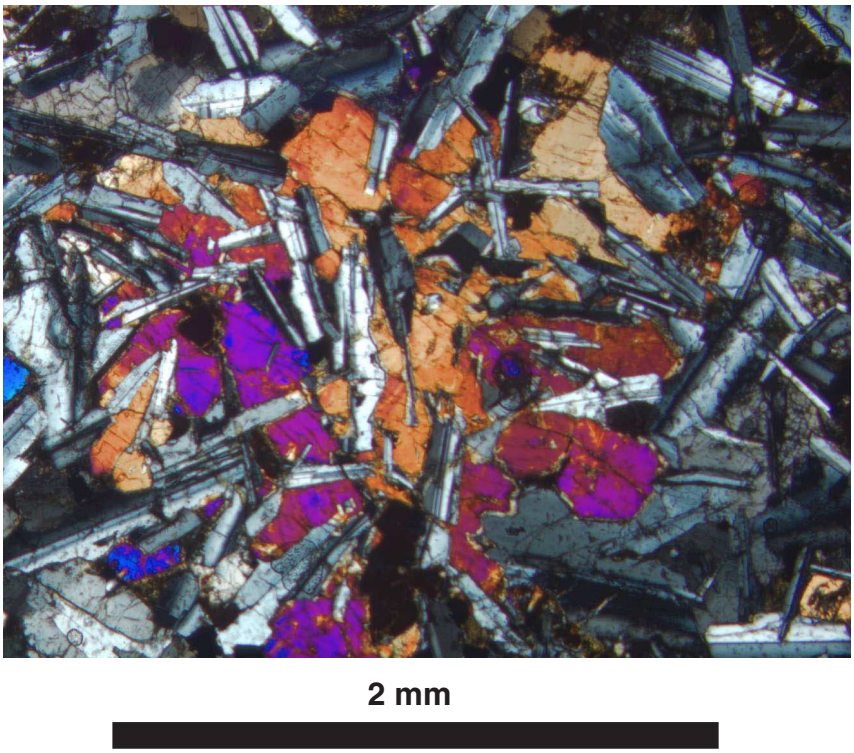

Figure F16. Photograph of interval 187-1161A-3R-1, 67–80 cm, showing fractures lined with cryptocrystalline silica within the chilled margin of a pillow fragment. The inner spherulitic zone of the pillow is highlighted as a result of partial replacement by clay.

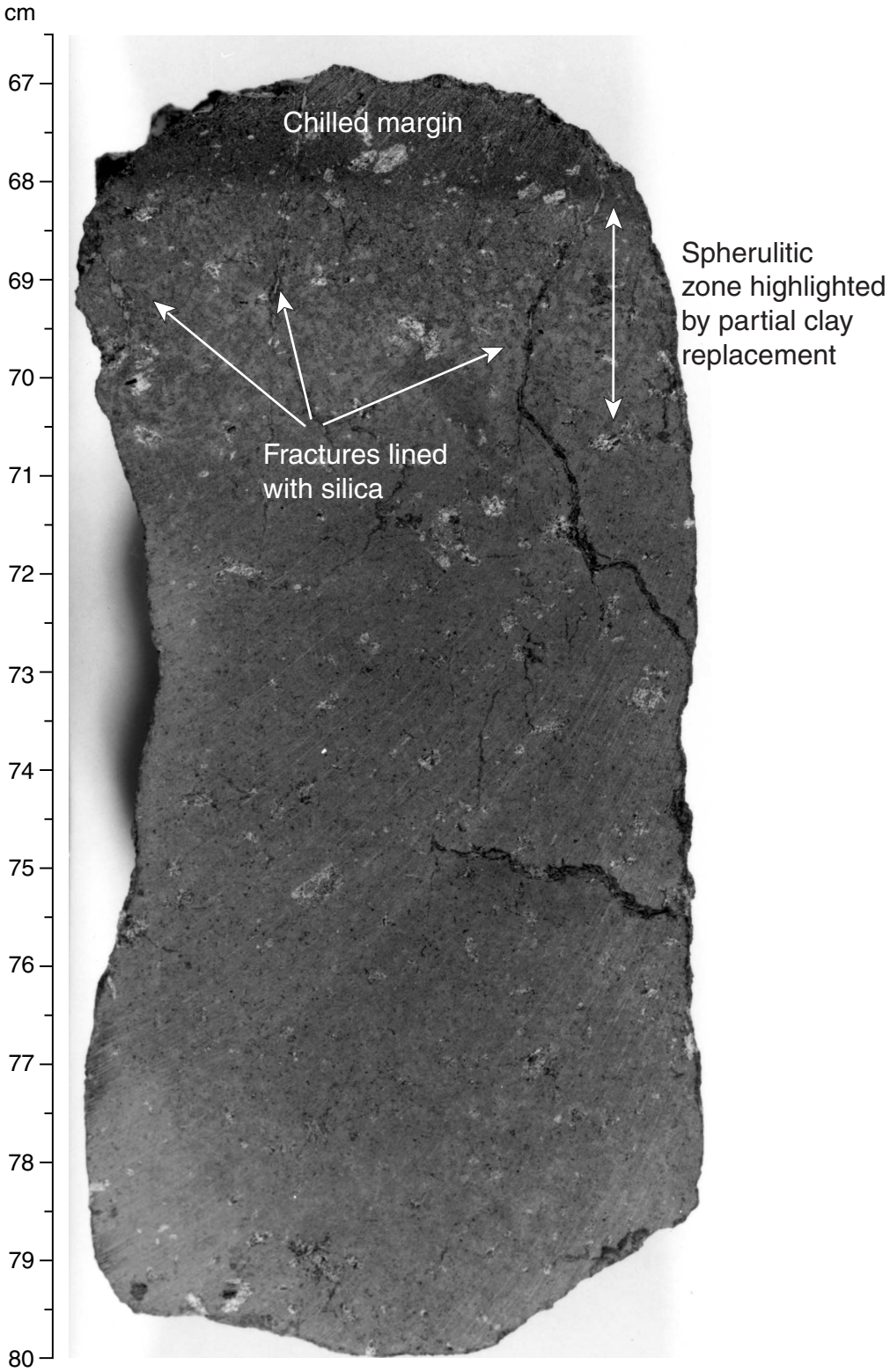

Figure F17. Photograph of interval 187-1153A-8R-1, 110–122 cm, showing a spherulitic pillow margin highlighted by Fe oxyhydroxide staining. Note the sediment fracture infill.

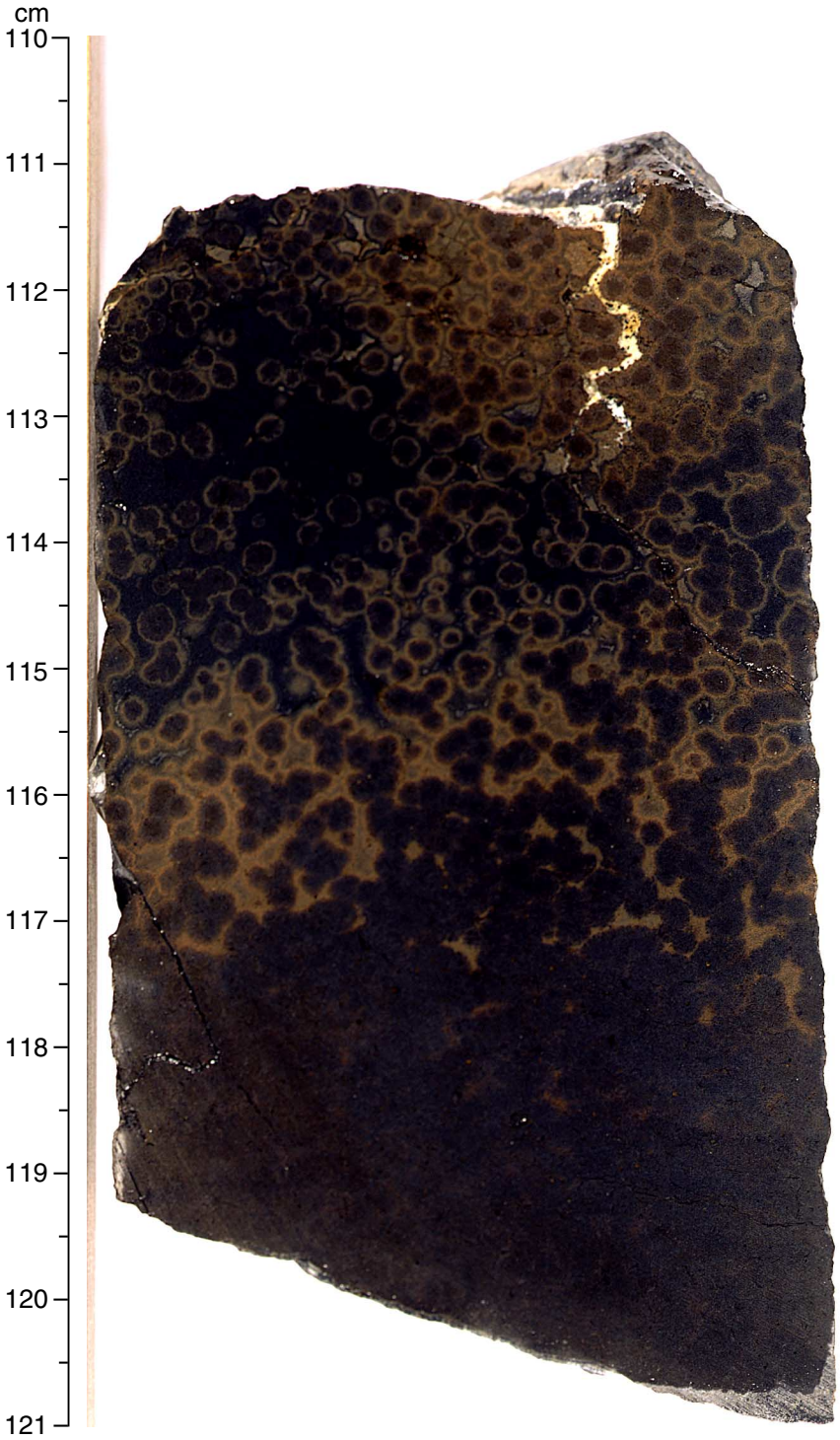

Figure F18. Photograph of interval 187-1152-6R-1, 33–40.5 cm, showing concentric alteration halos progressing from the more intensely altered margin to the less intensely altered interior of a sparsely phyric basalt. The alteration halo is thicker in the chilled margin at the top of the figure.

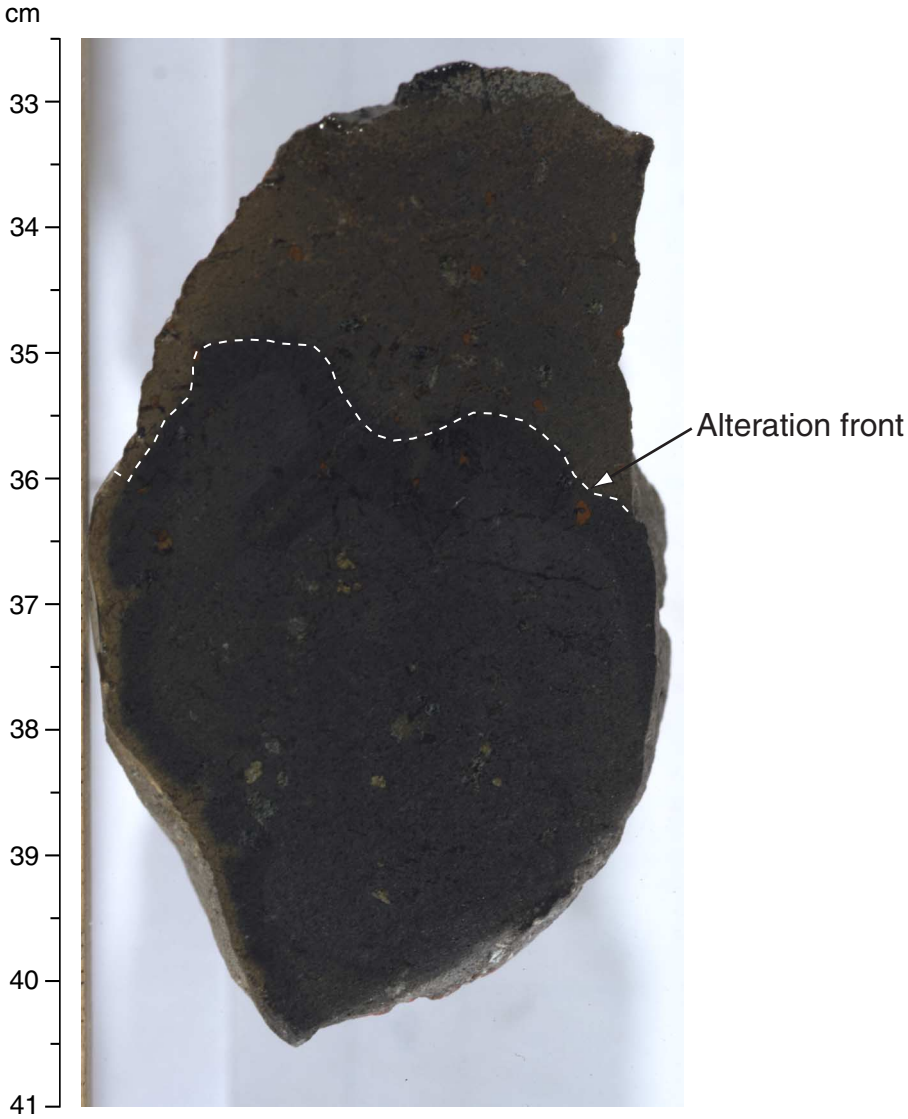

Figure F19. Photomicrograph, with crossed polars, of Sample 187-1156A-3R-2, 73–77 cm (see "Site 1156 Thin Sections," p. 26), showing the transition (left to right) from smectite and Fe oxyhydroxide groundmass replacement to virtually unaltered groundmass at the alteration halo boundary.

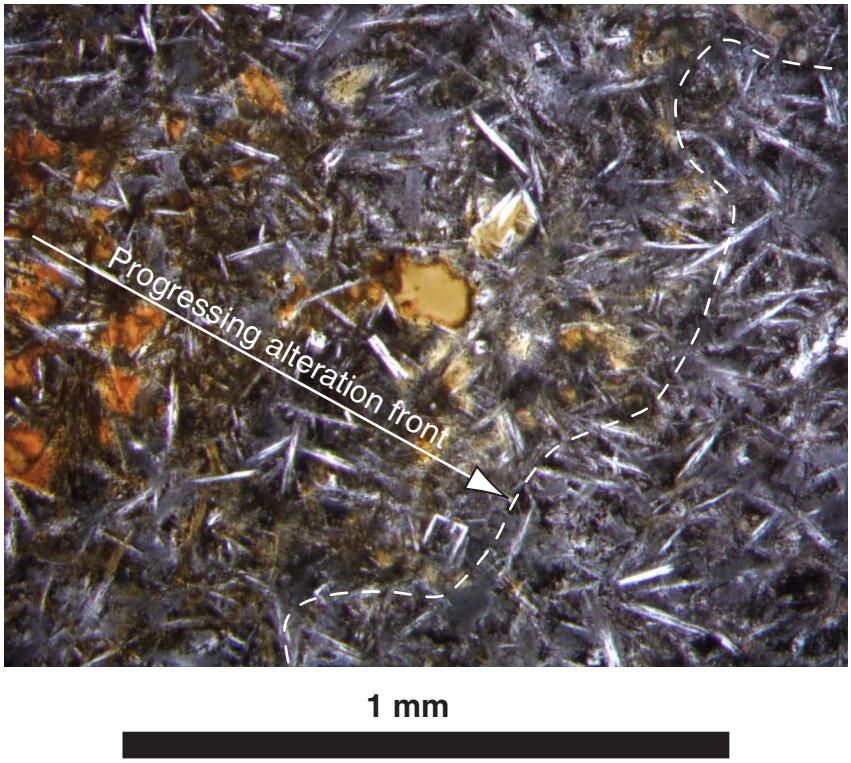

Figure F20. Photograph of Sample 187-1153A-8R-1, 102–106 cm, showing glassy pillow rind consisting of fresh glass, palagonite, and silica veins.

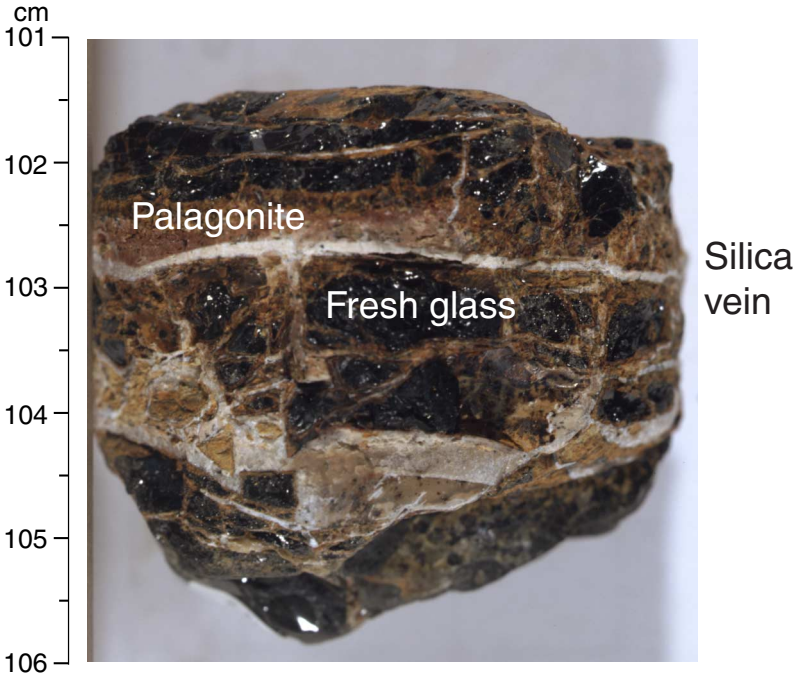

Figure F21. Photomicrograph of Sample 187-1155B-2R-1, 68–71 cm (see "Site 1155 Thin Sections," p. 31), showing the intersection of calcite veins with palagonite. Silica, Fe oxyhydroxides, and Mn oxide line the edge of the calcite vein. Palagonite is altered to clay along a dendritic alteration front associated with microbial degradation. The vertical fracture within the palagonite contains Mn-Fe oxyhydroxides and silica.

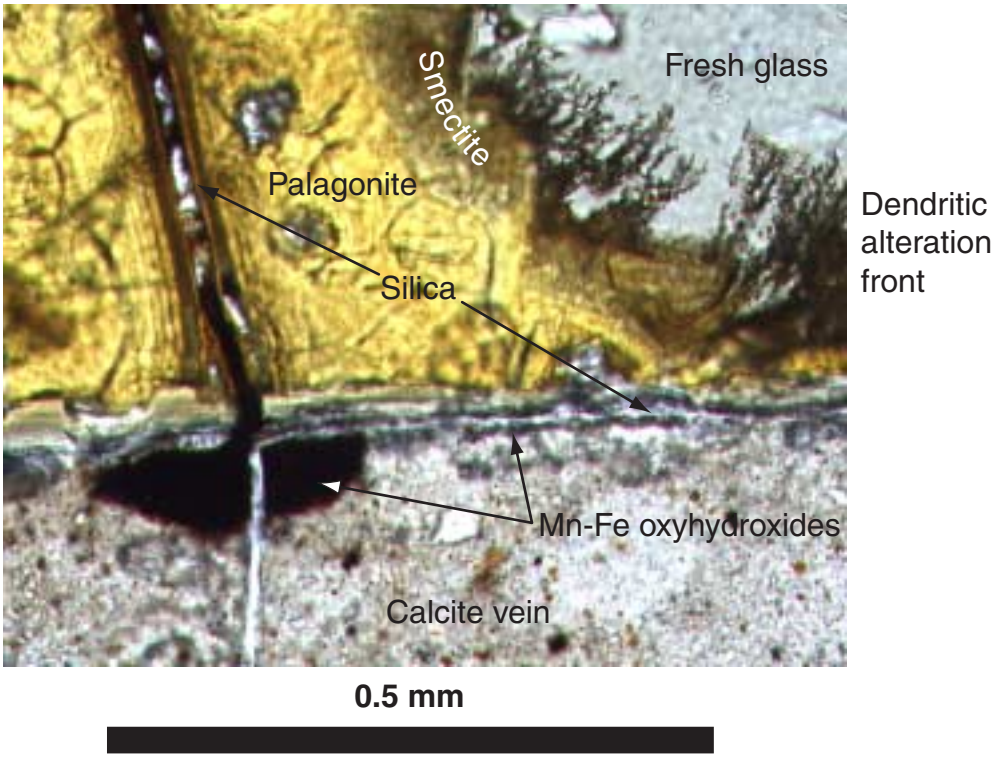

Figure F22. Photograph of interval 187-1157B-3R-1, 137–147 cm, showing calcite veins sporadically lined with thin silica selvages surrounded by symmetric alteration halos in which the groundmass and olivine phenocrysts are mostly replaced by smectite and Fe oxyhydroxide. Spotty Mn oxide is common within the calcite veins and along silica selvages.

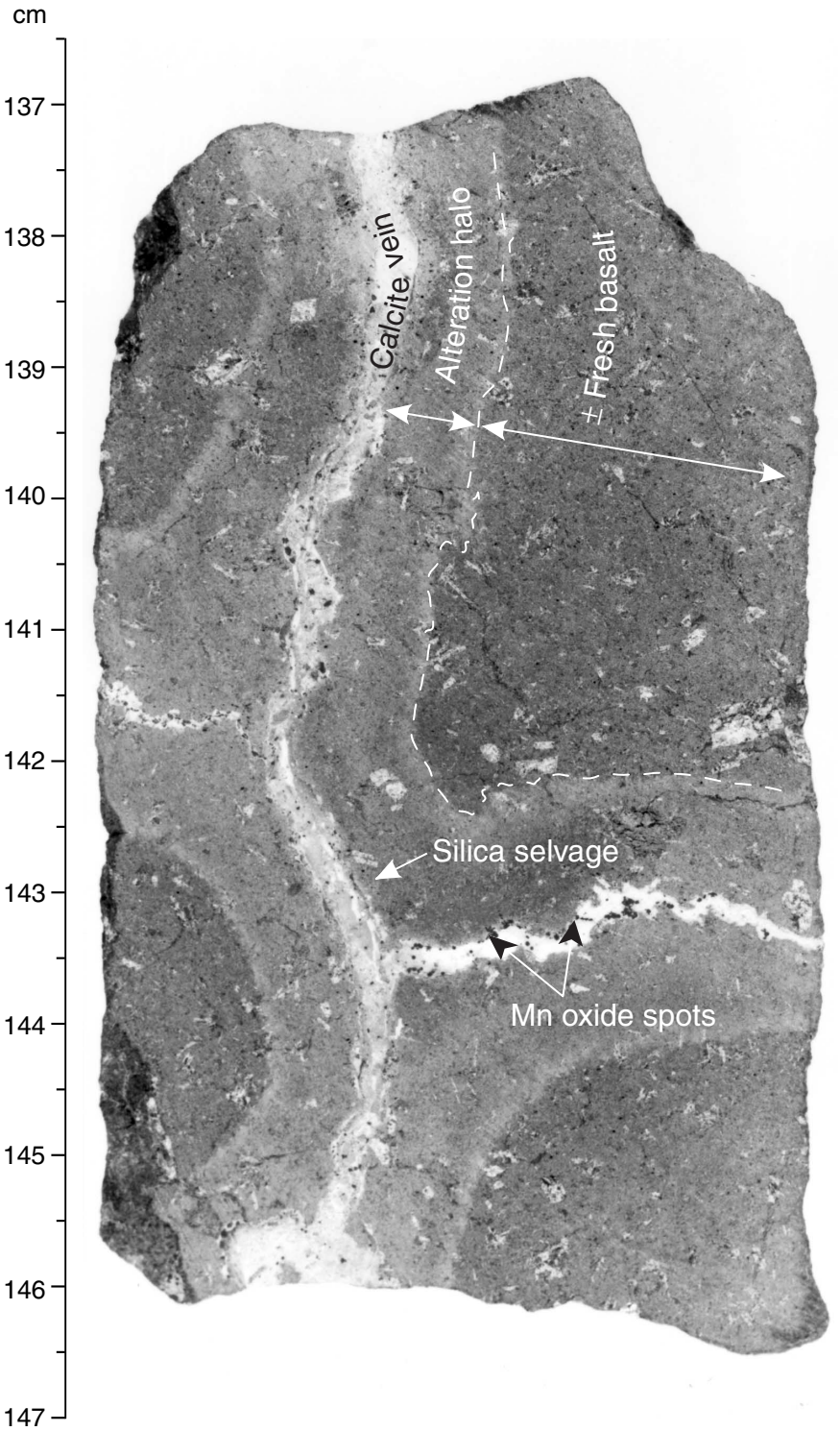

Figure F23. A. Variations in $^{206}Pb/^{204}Pb$ along the Southeast Indian Ridge (SEIR) between 115°E and 140°E. The present position of the isotope boundary between Indian- and Pacific-type provinces is located at ~126°E. Note the break in the horizontal scale due to the overlap of the AAD and Zone A axes (see Fig. F3, p. 21). Data are taken from Klein et al. (1988), Pyle et al. (1992), and Pyle et al. (1995). **B.** Variations of Zr/Ba vs. $^{206}Pb/^{204}Pb$ showing the data distribution used to determine Indian- and Pacific-type mantle provinces. Data are taken from Klein et al. (1988), Pyle et al. (1992, 1995), Pyle (1994), and D. Pyle and D. Christie (unpubl. data).

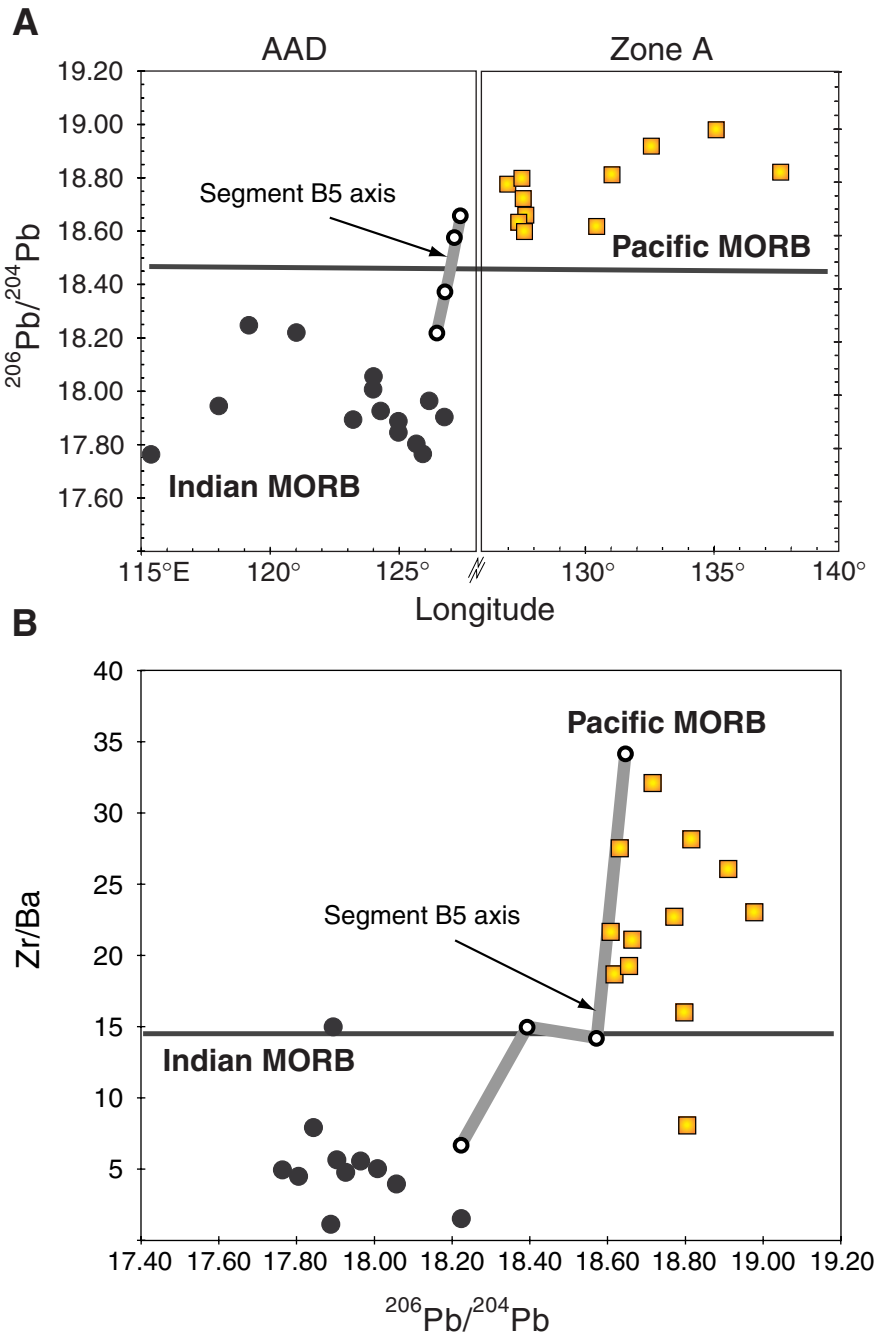

Figure F24. Distribution of MgO values in Hole 1160B. The hole passes through a sequence of seven flows in which pillow flows and massive flows alternate. Each massive flow is of the same lithology as the overlying pillow flow. Note the very similar high MgO contents of both glasses and massive flows. Whole-rock samples from the pillow flows have lost MgO during alteration.

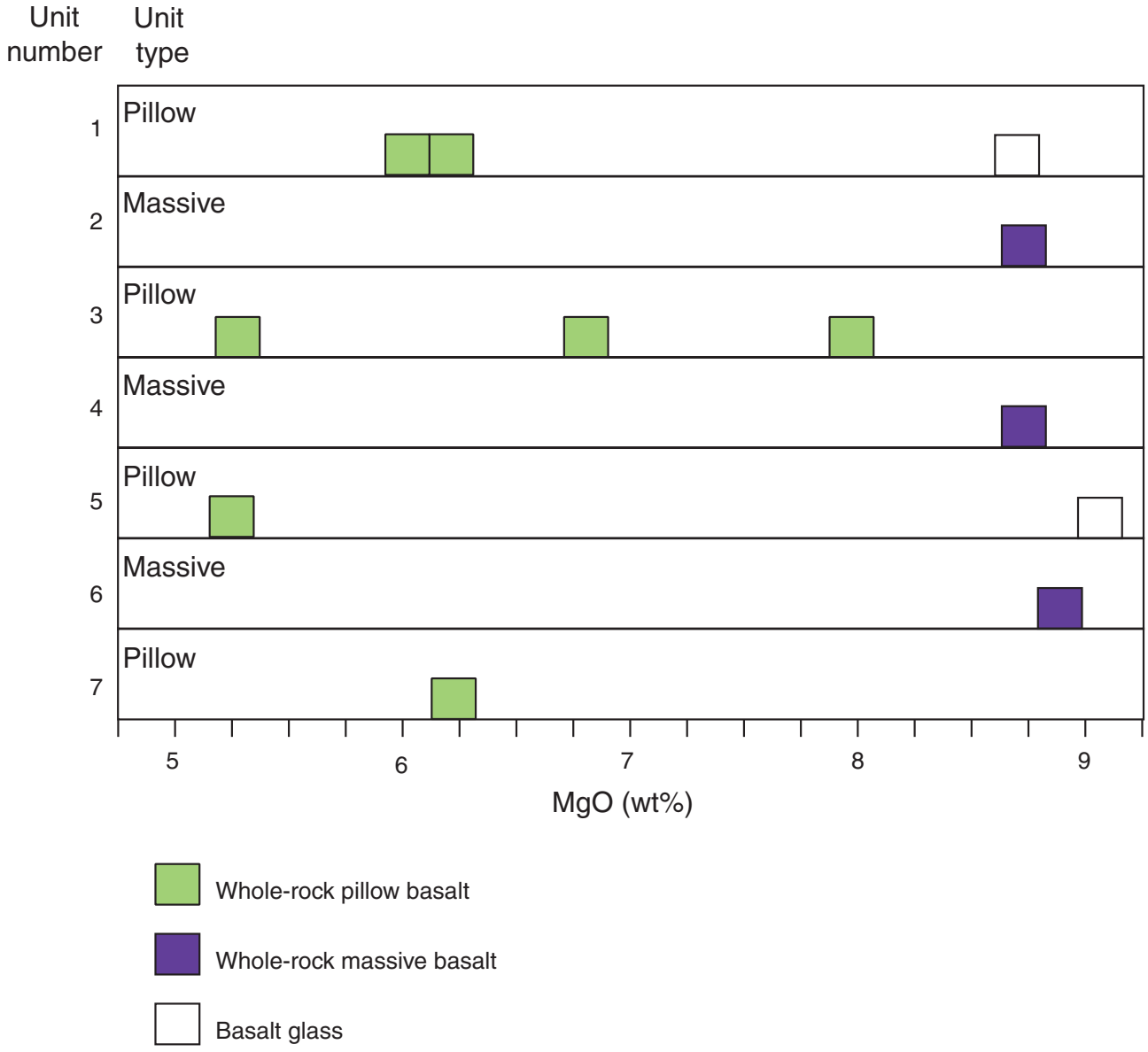

Figure F25. A. Variations in Zr/Ba vs. Ba of basaltic glasses dredged from 0- to 7-Ma seafloor within and east of the Australian Antarctic Discordance (AAD) (D. Pyle and D. Christie, unpubl. data). PRT = propagating rift tip lavas; dashed line = approximate geochemical boundary between Indian- and Pacific-type zero-age Southeast Indian Ridge basalt glass. **B.** Variations in Na_2O/TiO_2 vs. MgO of basaltic glass dredged from 0- to 7-Ma seafloor within and east of the AAD (D. Pyle and D. Christie, unpubl. data).

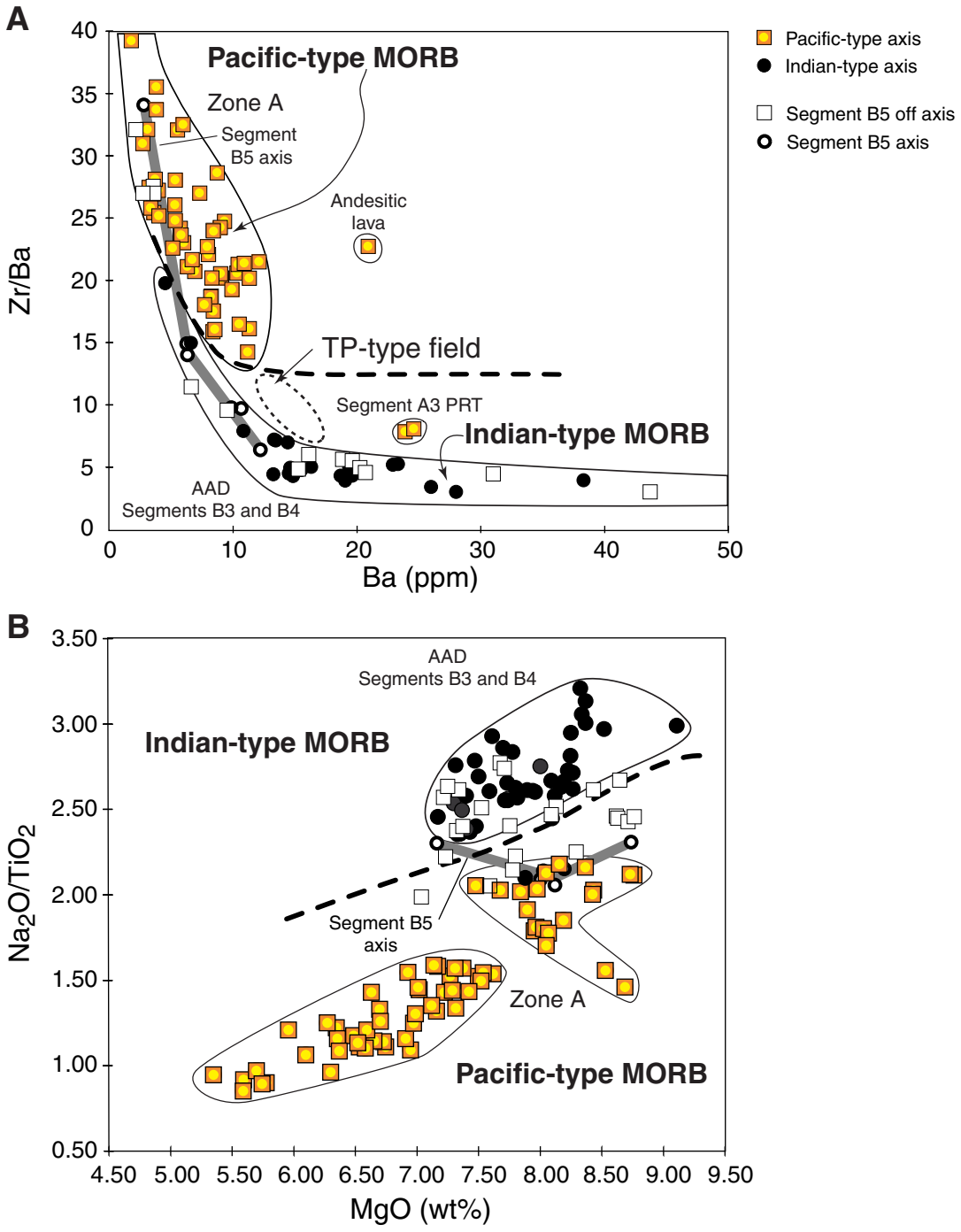

Figure F26. Analyses for all Leg 187 glasses in relation to the 0- to 7-Ma data fields from Figure F25, p. 43. Values plotted are averages of all shipboard replicates for each individual sample. **A.** Zr/Ba vs. Ba. Data are color coded according to the field in which they plot. Yellow triangles lie outside the 0- to 7-Ma fields and are referred to as Transitional Pacific (TP) because they appear to extend the Pacific field in the direction of Zone A propagating rift tip (PRT) lava compositions. The red triangle is a glass from Hole 1164A that plots at the boundary between the Pacific and Indian fields. **B.** Na_2O/TiO_2 vs. MgO. Color coding is defined by the Ba-Zr systematics in **A.** Note that no Leg 187 sample plots in the 0- to 7-Ma Indian field, but, with the exception of four Pacific samples, there is a clear division between Pacific and Indian samples. These four samples plot to the left of the Segment B5 tie line in **A**, a region where small analytical errors in Ba result in large shifts in plotting position. Note also that TP samples plot in both fields. Dashed line = approximate geochemical boundary between Indian- and Pacific-type zero-age Southeast Indian Ridge basalt glass.

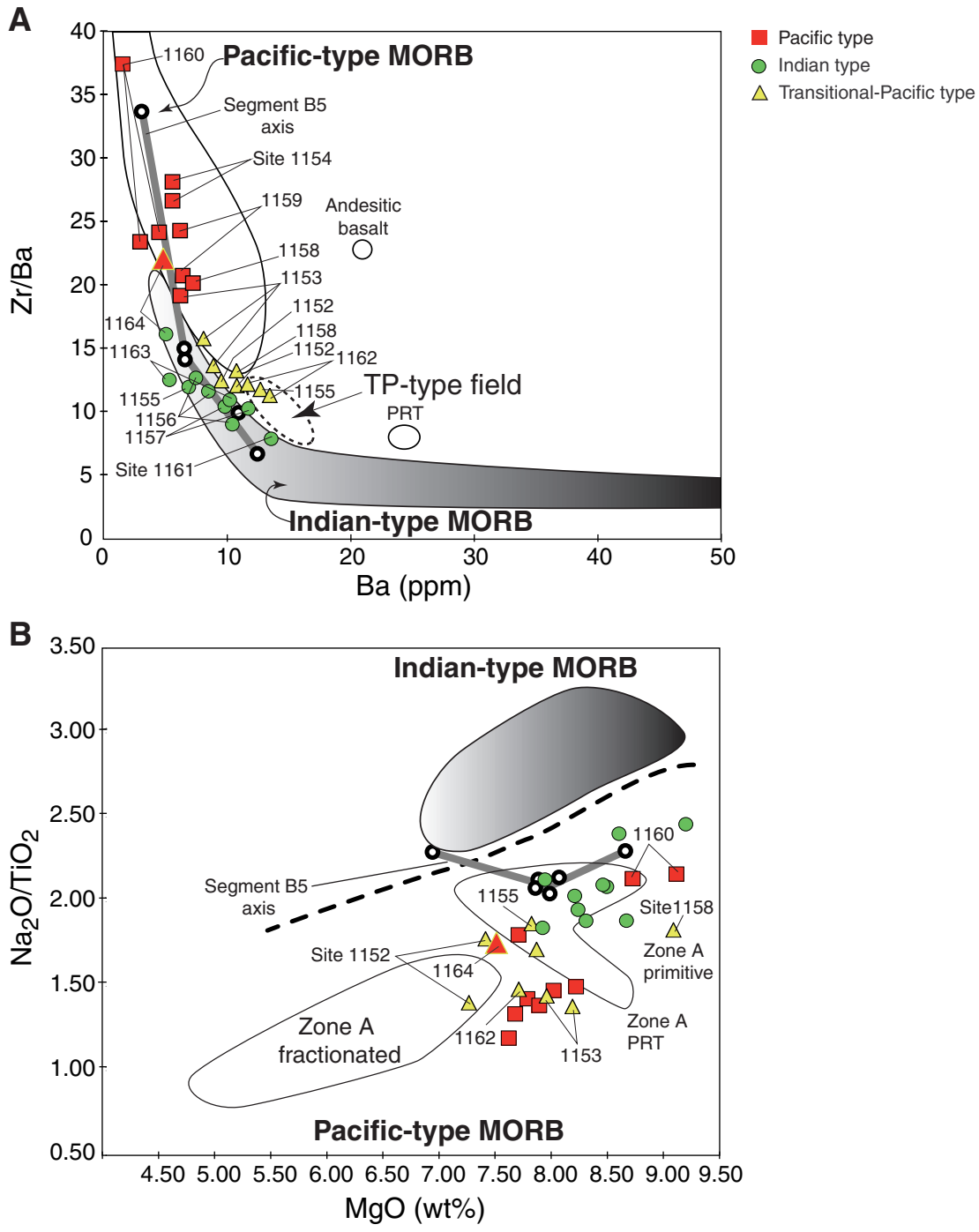

Figure F27. Leg 187 site locations in relation to seafloor isochrons (after Vogt et al., 1984). Sites are color coded according to the mantle domain interpreted from onboard Zr-Ba data based on Figure F26A, p. 44. Sites with two colors indicate that two mantle types were sampled. Colored lines are ship tracks for Leg 187 (blue) and the two site survey cruises aboard the *R/V Melville* (red and green).

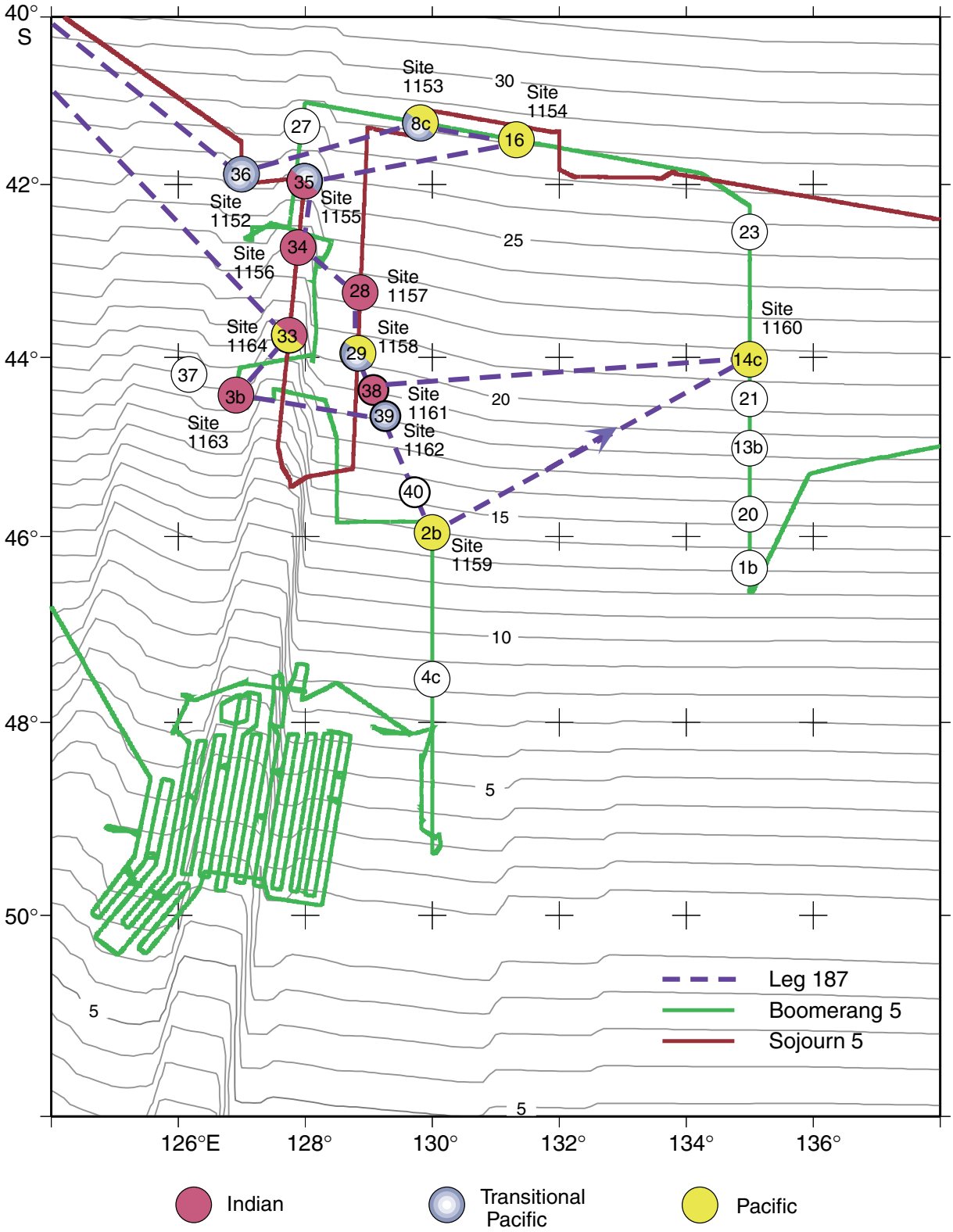

Figure F28. Leg 187 site locations in relation to the residual depth anomaly (gray contours) and SeaBeam bathymetry from the *R/V Melville* Boomerang 5 and Sojourner 5 site survey cruises. Site colors are as in Figure F27, p. 45. The base map is after Christie et al. (1998).

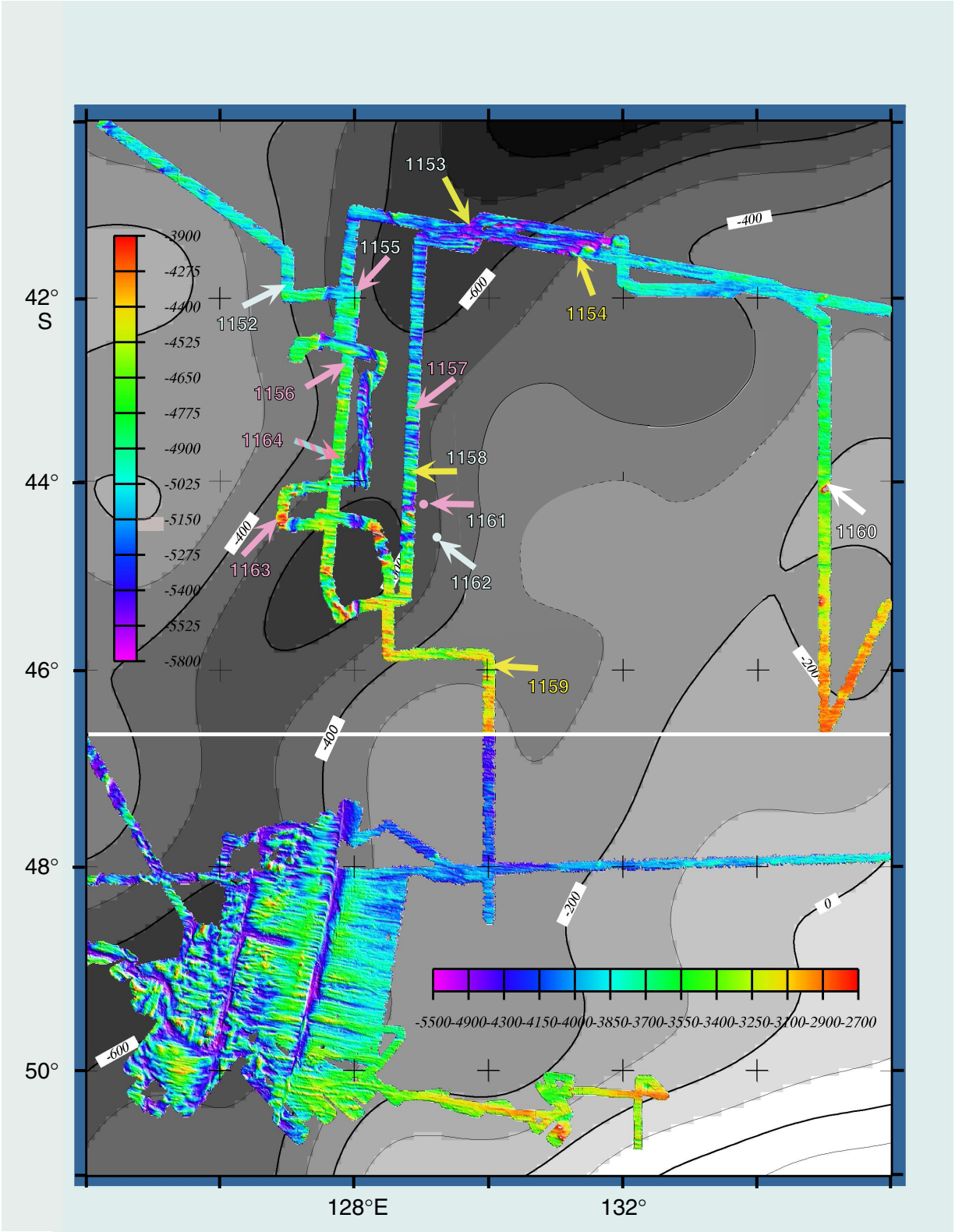

Table T1. Coring summary, Leg 187.

Hole	Latitude	Longitude	Water depth (m)	Number of cores	Interval cored (m)	Recovered		Drilled (m)	Maximum penetration (m)	Time on hole (hr)
						Core (m)	(%)			
1152A	41°53.9′S	127°0.4′E	5055.4	1	11.2	0.59	5.3	0	11.2	0
1152B	41°53.8′S	127°0.5′E	5055.4	5	23.7	3.59	15.1	22.6	46.3	36.8
		Site 1152 totals:		6	34.9	4.18	12.0	22.6	46.3	36.8
1153A	41°16.3′S	129°48.9′E	5581.4	1	7.3	1.77	24.2	267.6	274.9	67.0
		Site 1153 totals:		1	7.3	1.77	24.2	267.6	274.9	67.0
1154A	41°28.7′S	131°19.0′E	5736.4	8	34.4	9.42	27.4	233.2	267.6	75.0
		Site 1154 totals:		8	34.4	9.42	27.4	233.2	267.6	75.0
1155A	41°57.5′S	127°59.7′E	4975.4	6	26.2	2.34	8.9	177.3	203.5	53.5
1155B	41°57.5′S	127°59.5′E	4975.4	9	46.0	18.18	39.5	147.9	193.9	51.5
		Site 1155 totals:		15	72.2	20.52	28.4	325.2	203.5	105.0
1156A	42°44.0′S	127°53.3′E	4867.3	2	11.4	6.30	55.3	118.2	129.6	32.0
1156B	42°43.9′S	127°53.3′E	4867.3	5	33.6	9.92	29.5	181.6	215.2	42.0
		Site 1156 totals:		7	45.0	16.22	36.8	299.8	215.2	74.0
1157A	43°15.7′S	128°53.2′E	5069.3	3	16.4	2.92	17.8	200.0	216.4	28.0
1157B	43°15.7′S	128°53.0′E	5069.3	8	40.4	11.70	29.0	130.6	171.0	46.0
		Site 1157 totals:		11	56.8	14.62	25.7	330.6	216.4	74.0
1158A	43°56.9′S	128°49.7′E	5167.3	2	14.4	0.85	5.9	198.9	213.3	26.5
1158B	43°56.8′S	128°49.7′E	5167.3	3	15.0	1.60	10.7	126.2	141.2	16.3
1158C	43°56.7′S	128°49.7′E	5167.3	1	9.4	1.61	17.1	108.0	117.4	17.8
		Site 1158 totals:		6	38.8	4.06	10.5	433.1	213.3	60.6
1159A	45°57.4′S	129°60.0′E	4504.2	6	27.7	7.96	28.7	145.6	173.3	68.5
		Site 1159 totals:		6	27.7	7.96	28.7	145.6	173.3	68.5
1160A	44°0.6′S	134°59.9′E	4625.2	2	5.1	0.43	8.4	166.0	171.1	38.8
1160B	44°0.5′S	134°59.9′E	4625.2	8	45.1	13.01	28.8	160.1	205.2	43.3
		Site 1160 totals:		10	50.2	13.44	26.8	326.1	205.2	82.1
1161A	44°17.2′S	129°3.1′E	5020.1	4	29.3	4.39	15.0	116.0	145.3	55.3
1161B	44°17.1′S	129°3.1′E	5020.1	2	8.5	0.86	10.1	158.5	167.0	20.3
		Site 1161 totals:		6	37.8	5.25	13.9	274.5	312.3	75.6
1162A	44°38.0′S	129°11.3′E	5464	4	31.4	2.58	8.2	333.2	364.6	39.5
1162B	44°37.9′S	129°11.3′E	5464	10	58.9	9.94	16.9	348.4	407.3	61.0
		Site 1162 totals:		14	90.3	12.52	13.9	681.6	407.3	100.5
1163A	44°25.5′S	126°54.5′E	4354	10	47.1	15.70	33.3	161.0	208.1	65.5
		Site 1163 totals:		10	47.1	15.70	33.3	161.0	208.1	65.5
1164A	43°44.9′S	127°44.9′E	4798	3	8.5	0.97	11.4	138.5	147.0	27.8
1164B	43°45.0′S	127°44.8′E	4798	9	65.7	10.65	16.2	150.4	216.1	45.8
		Site 1164 totals:		12	74.2	11.62	15.7	288.9	216.1	73.6
Leg 187 totals:				112	616.7	137.28	22.3	3789.8	407.3	957.8

Note: This table is also available in **ASCII** format.

Table T2. Summary of igneous petrology, Leg 187. (See table notes. Continued on next page.)

Age (Ma)	Hole	Mantle domain	Length (m) Cored	Length (m) Recovered	Recovery (%)	Igneous lithology: Aphyric	Sparsely pl-ol phyric	Moderately pl-ol phyric	Breccia	Deposit type	Unit name	Alteration
~25	1152A	Transitional Pacific	11.20	0.60	5.00	X				Talus	Unit 1: Aphyric basalt	Slight
	1152B	Transitional Pacific	23.70	3.60	15.15	X	(x)	X (cpx)		Talus	Unit 1: Aphyric basalt	Slight
										Talus	Unit 2: Sparsely to moderately pl-ol-cpx phyric basalt	Slight
			Total:	4.20	12.03							
~28	1153A	Pacific	7.30	1.77	24.25	X				Pillows	Unit 1: Aphyric basalt	Slight
			Total:	1.77	24.25							
~28	1154A	Pacific	34.40	9.42	28.90			X		Pillows	Unit 1: Moderately pl-ol phyric basalt	Slight
			Total	9.42	28.90							
~24.5	1155A	Transitional Pacific	26.20	2.34	8.93	X	(X)	X		Pillows	Unit 1: Sparsely to moderately pl-ol phyric basalt	Slight to moderate
										Talus	Unit 2: Aphyric basalt	
	1155B	Transitional Pacific	46.00	18.18	39.52			X	CCV	Pillows into sediments	Unit 1: Moderately pl-ol phyric basalt (micritic sediments + lithics in fractures)	High at top Slight at bottom
			Total:	20.52	28.42							
~22	1156A	Indian	11.40	6.30	55.26		(x)	X	X (Cc) CCV	Talus Pillows	Unit 1: Breccia of phyric basalt Unit 2: Sparsely to moderately pl-ol phyric basalt with carbonate sediments	Slight Slight to moderate
	1156B	Indian	33.60	9.92	29.52			X		Unknown	Unit 1: Moderately to highly pl-ol phyric basalt	Slight to moderate
			Total:	16.22	36.04							
~22.5	1157A	Indian	16.40	2.92	17.80	X		X	X (Cc) CCV	Rubble	Unit 1: Basaltic rubble (aphyric and pl-ol phyric basalt with carbonate sediments)	Slight to moderate
	1157B	Indian	40.40	11.70	28.96			X		Pillows	Unit 1: Moderately pl-ol phyric basalt	Slight to moderate
			Total:	14.62	25.74							
~21	1158A	Pacific	14.40	0.85	5.90	X	X			Rubble (pillows)	Unit 1: Aphyric to sparsely ol-pl phyric basalt (fine grained)	Slight to moderate
	1158B	Pacific	15.00	1.60	10.67	X	X			Rubble? (flow/dike)	Unit 1: Aphyric to sparsely ol-pl phyric basalt (fine grained)	Slight to moderate
	1158C	Pacific	9.40	1.61	17.13	X	X			Flow/dike?	Unit 1: Aphyric to sparsely ol-pl phyric basalt Unit 2: Diabase (with aphyric basalt)	Slight to moderate Moderate to high
			Total:	4.06	10.33							
~14	1159A	Pacific	27.70	7.96	28.74	X			X (Si)	Pillows	Unit 1: Aphyric basalt (+ hyaloclastites)	Slight to moderate
			Total:	7.96	28.74							
~21.5	1160A	Pacific	5.10	0.43	8.43	X		X		Rubble (pillows)	Unit 1: Aphyric basalt	Slight to moderate
	1160B	Pacific	45.10	13.01	28.85	X		X		Pillows	Unit 1: Aphyric basalt (microcrystalline)	Moderate
										Massive	Unit 2: Aphyric basalt (fine grained)	Slight
										Pillows	Unit 3: Moderately pl-(ol) basalt (microcrystalline)	Moderate to high
										Massive	Unit 4: Moderately pl ± ol phyric basalt (fine grained)	Slight
										Pillows	Unit 5: Moderately pl-ol basalt (microcrystalline)	Moderate to high
										Massive	Unit 6: Moderately pl phyric basalt (fine grained)	Slight to moderate
										Pillows	Unit 7: Aphyric basalt (microcrystalline)	Slight
			Total:	13.44	26.77							
~19	1161A	Indian	29.30	4.39	14.98	X	X	X	X (Si)	Talus	Unit 1: Basaltic rubble (sparsely pl-ol phyric basalt; moderately pl-ol phyric basalt; fine-grained aphyric basalt with Si-clay cemented breccia)	Moderate to high
	1161B	Indian	8.50	0.86	10.12	X	X	X	X (Si)	Talus	Unit 1: Basaltic rubble (microcrystalline aphyric basalt; sparsely pl-ol phyric basalt; moderately pl-ol phyric basalt; fine-grained aphyric basalt with Si-clay cemented breccia)	Moderate to high
			Total:	5.25	13.89							

Table T2 (continued).

Age (Ma)	Hole	Mantle domain	Length (m) Cored	Length (m) Recovered	Recovery (%)	Igneous lithology: Aphyric	Sparsely pl-ol phyric	Moderately pl-ol phyric	Breccia	Deposit type	Unit name	Alteration
~18	1162A	Pacific	31.40	2.58	8.22	X?	?	X?	X (Dc)	Fault Breccia?	Unit : Mixed igneous clasts (metabasalt) Unit 2: Dolomite-cemented breccia (basalt, metadiabase, cataclasite)	High to very high High to very high
	1162B	Pacific	58.90	9.94	16.88	X?	?	X?	X (Dc)	Fault Breccia?	Unit 1: Dolomite limestone (with lithics) Unit 2: Dolomite-cemented breccia (aphyric and phyric basalt)	High to very high High to very high
			Total:	12.52	13.86							
~17	1163A	Transitional Pacific	47.10	15.70	33.33	X		X	X (Cc) CCV	Pillows	Unit 1: Moderately pl-ol phyric basalt Unit 2: Aphyric basalt with carbonate sediments	Slight to moderate Slight to moderate
			Total:	15.70	33.33							
18–19	1164A	Transitional Pacific	8.50	0.97	11.41	X (cpx)				Pillows	Unit 1: Aphyric basalt (pl-cpx microphyric)	Slight
	1164B	Transitional Pacific	65.70	10.65	16.21	X	X	X	X (Si)	Rubble (pillows)	Unit 1: Basaltic rubble (aphyric and pl-ol phyric basalt with Si-clay cemented breccia)	Slight to high
			Total:	11.62	15.66							
		Cruise totals:	617.20	137.30	22.25							

Notes: pl-ol = plagioclase-olivine; X = was definitely present; (x) = small amount was present; cpx = clinopyroxene; CCV = composite calcite vein; (Cc) = calcite; X? = metamorphosed or highly altered clasts of uncertain mineralogy; ? = uncertain due to alteration; (Dc) = dolomite. This table is also available in **ASCII** format.